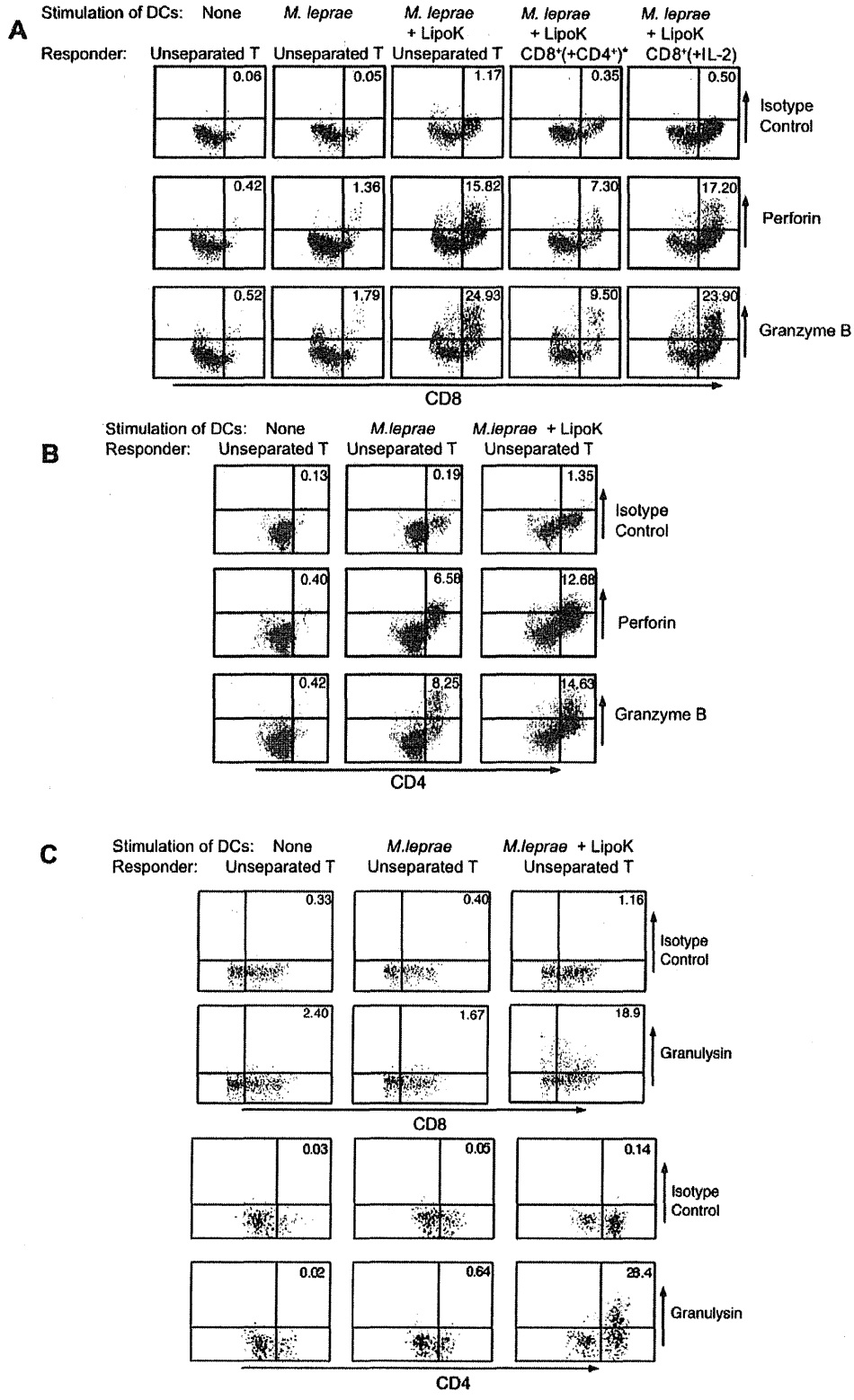

Figure 4. Production of perforin, granzyme B and granulysin in CD8$^+$ T cells as well as CD4$^+$ T cells. (**A**) Enhanced production of perforin and granzyme B from CD8$^+$ T cells cultured with LipoK stimulated *M. leprae* infected DCs. Intracellular staining of perforin and granzyme B was performed as follows: Cells were first stained with PE conjugated anti-CD4 or APC conjugated anti-CD8 mAb. Then, the cells were fixed in 2%

formaldehyde, permeabilized in 0.1% saponin, and stained with FITC conjugated anti-perforin mAb or anti-granzyme B mAb or isotype control IgG2a. Figure shows the dot plot of the gated $CD8^+$ T cells. The right hand quadrant shows $CD8^{high}$ T cells (activated $CD8^+$ T cells) and the number indicates the percentage of perforin or granzyme B positive T cells among gated $CD8^{high}$ T cells. *To determine whether direct interaction between $CD4^+$ and $CD8^+$ T cells for perforin and granzyme B production from $CD8^+$ T cells, is needed, $CD4^+$ T cells were cultured in inserts in a 24-well plate, and were not allowed to interact directly with $CD8^+$ T cells. As a control experiment, exogenous IL-2 (in the left hand dot plot) at a concentration of 50 U/ml was added to $CD8^+$ T cells. (**B**) Enhanced expression of perforin and granzyme B from $CD4^+$ T cells. The right hand quadrant shows $CD4^{high}$ T cells, and the number indicates percentage of $CD4^{high}$ T cells producing perforin and granzyme B. (**C**) Enhanced expression of granulysin from $CD8^+$ and $CD4^+$ T cells, co-cultured with LipoK and *M. leprae* stimulated DCs. The protocol was followed as per the staining of perforin, except that the surface stain used was FITC conjugated-CD4 and APC conjugated anti-CD8 mAb, and subsequently PE conjugated granulysin was used. Figure shows the dot plot of the gated $CD8^+$ and $CD4^+$ T cells. The right hand quadrant shows $CD8^{high}$ or $CD4^{high}$ T cells (activated T cells) and the number indicates the percentage of granulysin positive T cells among gated $CD8^{high}$ and $CD4^{high}$ T cells. Representative data of three separate experiments with different donors is shown.
doi:10.1371/journal.pntd.0001401.g004

antibody could almost totally inhibit the IL-12 production from DCs, as well as the T cell activating function of DCs (not shown), probably through blocking of the classical NF-kB pathway. Indeed, parthenolide, one of the major sesquiterpene lactones, known to inhibit NF-kB activity [24], inhibited the IL-12 production from DCs stimulated with *M. leprae* and LipoK. Also, IL-12 was efficiently produced when *M. leprae* was viable and not dead. Thus, although the exact mechanisms remain to be elucidated, some cell surface molecules and secreted components of *M. leprae* are responsible for the production of IL-12, which further modulates type 1 T cell responses [32,33].

A number of mechanisms are known to be involved in the clearance of intracellular bacteria, such as IFN-γ release, apoptosis induction of the macrophages and anti-microbial activity of CTL [12,15]. Production of IFN-γ could boost the ability to kill pathogens in host cells. In fact, it was found that LipoK activated *M. leprae* infected DCs, highly stimulated both memory $CD4^+$ and $CD8^+$ T cells, as well as naïve $CD4^+$ to produce IFN-γ, and further assisted in the proliferation of both T cell subsets (Fig. 3).

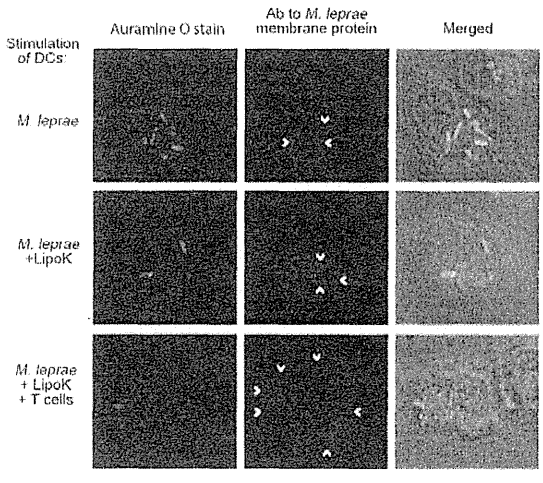

Figure 5. Localization of the membrane components of *M. leprae* at the periphery of the DCs. DCs were infected with either *M. leprae* alone or further stimulated with LipoK for 2 days and in some cases co-cultured with T cells. After 3 days co-culture with T cells, cover glass with attached DCs were fixed and observed under confocal microscopy-LSM5 Exciter. *M. leprae* was stained with Auramine O (shown in green) and *M. leprae* membrane components were stained with polyclonal rabbit antibody raised against the membrane fraction of *M. leprae* (depicted in red fluorescence). Alexa Fluor 633 conjugated anti-rabbit antibody (Molecular Probes) was used as the secondary antibody. Arrowheads indicate the positively stained region. Experiments were performed twice with different donors.
doi:10.1371/journal.pntd.0001401.g005

Inhibition of MHC class I and class II molecules on DCs, indicated that the activation of these T cells were MHC class II- and class I-dependent in $CD4^+$ T cell and $CD8^+$ T cells respectively. Further, proteolytic processing of *M. leprae* antigens was probably enhanced by LipoK treatment of DCs, since incubation with anti-*M. leprae* membrane Ab showed positive staining at the periphery of DCs, when co-cultured with T cells (Fig. 5). In addition, preliminary results showed that expression of MHC class I and II molecules on LipoK activated DCs, were elevated in those co-cultured with T cells. Thus, LipoK could probably assist in the processing and presentation of *M. leprae* antigens, and thereby, highly activate T cells.

The other important parameter, for the clearance of mycobacteria from the host cell, is their potential to activate antimicrobial effector mechanisms in human T cells. DCs have been shown to be involved in CTL induction following uptake of antigenic particles [25,34,35,36]. $CD8^+$ T cells co-cultured with LipoK

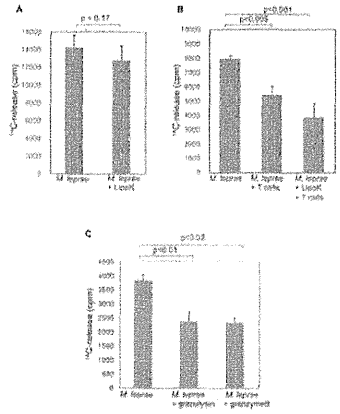

Figure 6. Reduction in the viability of *M. leprae* in DCs after co-culture with T cells and LipoK stimulation. (**A**) DCs were infected with *M. leprae* and stimulated with LipoK, 2 days later, cells were collected and the viability of *M. leprae* in DCs was measured by the radiorespirometric assay (metabolic CO_2 release) as described in Materials and Methods. In brief, ^{14}C labeled palmitic acid was added to the lysates of DCs and cultured at 33°C. After 7 days of culture, the amount of $^{14}CO_2$ evolved was measured using a Packard 1500 TRI-CARB liquid scintillation analyzer. (**B**) DCs were infected with *M. leprae* as in **A**, and co-cultured with T cells. Six days after the co-culture, DCs were lysed, and the viability of *M. leprae* was determined by the radiorespirometric assay. (**C**) *M. leprae* at a concentration of 1×10^7/well/200 µl in Middlebrook 7H9 media was incubated with granulysin or granzyme B for a period of 3 days at 33°C, and the viability determined as described in **A**. Unpaired Student's t test was used to find the statistical significance of the two sets of data. Representative data of three separate experiments is shown.
doi:10.1371/journal.pntd.0001401.g006

stimulated *M. leprae*-infected DCs, through $CD4^+$ T cells' help produced increased amount of cytolytic effector molecules: perforin and granzyme B. Adequate production of these cytolytic proteins from $CD8^+$ T cells required direct contact with $CD4^+$ T cells. Recently, there are studies that certain types of $CD4^+$ T cells possess direct cytotoxic potential [25,37,38]. We observed a portion of $CD4^{high}$ T cells (activated T cells), have the capacity to produce cytotoxic granules. Bastian et al. demonstrated that native *M. tuberculosis* heterogenous lipopeptides are potent immunogens for primary human T cells, and those T cells were $CD4^+$ and MHC class II restricted, challenging the current concepts that cytotoxic T cells were restricted to $CD8^+$ T cell subset [25]. Another lytic molecule, present in cytotoxic granules of T cells, is granulysin, which is reported to have direct anti-bacterial activity. Reports have shown the ability of T cells to secrete granulysin at the site of *M. leprae* infection, which provides evidence that anti-microbial activity of granule containing T cells is a mechanism of host defense in leprosy [39,40]. We observed that LipoK stimulated, *M. leprae* infected DCs, highly enhanced the production of granulysin from $CD8^+$ T cells. Unexpectedly, we observed that the percentage of $CD4^+$ T cells producing granulysin was higher than $CD8^+$ T cells. But, this fact was in lines with the earlier data, which showed co-localization of granulysin and $CD4^+$ T cells in tuberculoid leprosy lesions [39,40]. Thus, granulysin release by LipoK-mediated activation process, may lead to a direct anti-microbial effector pathway of host defense. These data demonstrated that both $CD4^+$ T cells and $CD8^+$ T cells, contribute to the induction of intracellular killing of *M. leprae*. These speculations were further supported by the fact that 50% of the phagocytosed bacilli were killed when infected DCs stimulated with LipoK, were co-cultured with T cells. This is the first observation of killing of *M. leprae* in an *ex vivo* system using human DCs and T cells. To further provide evidence of the effector mechanism at work during *M. leprae* killing by CTL, the direct effect of granulysin on *M. leprae* killing *in vitro* was analyzed. Results indicated that about 40% of *M. leprae* was killed by granulysin. Granulysin could probably lyse *M. leprae* by binding to the lipidic cell wall, through the same mechanism by which *M. tuberculosis* is destroyed by granulysin. Since, perforin is an essential molecule in the killing of intracellular *M. tuberculosis* [16], similar operation may be involved in intracellular *M. leprae* killing since perforin was effectively produced by T cells in our CTL culture system. On the other hand, direct killing of mycobacteria by granzymes is not known. But the viability of *M. leprae* was significantly lowered by granzyme B. Since granzyme B is one of the serine proteases that can target cytosolic and nuclear substrates to induce host cell death through mitochondrial perturbation, it may be involved in destroying the cell wall architecture of *M. leprae* by still unknown mechanism [41,42]. The contribution of the cytotoxic granules to killing of bacteria remains to be of interest for further investigation. Together, the results indicate that LipoK could contribute to protective host response against leprosy and eventually kill the bacteria, through the production of perforin, granulysin and granzyme B in T cells.

Acknowledgments

We appreciate the helpful assistance of Drs. Masanori Matsuoka and Masaichi Gidoh for the *M. leprae* propagation and isolation. Technical help for ELISA was kindly provided by Yukie Harada, Mizuho Kujiraoka, and Kumiko Matsubara for the isolation of PBMCs. We also thank the Japanese Red Cross Society for kindly providing the whole blood cells from healthy donors.

Author Contributions

Conceived and designed the experiments: YM TT YF MM. Performed the experiments: YM TT YF. Analyzed the data: YM TT TM MK MM. Contributed reagents/materials/analysis tools: YM TM MK. Wrote the paper: YM TT MM.

References

1. World Health Organization (2010) Global leprosy situation. Weekly epidemiological record 35: 337–348.
2. Ridley DS, Jopling WH (1966) Classification of leprosy according to immunity. A five-group system. Int J Lepr Other Mycobact Dis 34: 255–273.
3. Kaplan G, Cohn ZA (1986) The immunobiology of leprosy. Int Rev Exp Pathol 28: 45–78.
4. Maeda Y, Makino M, Crick DC, Mahapatra S, Srisungnam S, et al. (2002) Novel 33-kilodalton lipoprotein from *Mycobacterium leprae*. Infect Immun 70: 4106–4111.
5. Yamashita Y, Maeda Y, Takeshita F, Brennan PJ, Makino M (2004) Role of the polypeptide region of a 33 kDa mycobacterial lipoprotein for efficient IL-12 production. Cell Immunol 229: 13–20.
6. Tschumi A, Nai C, Auchli Y, Hunziker P, Gehrig P, et al. (2009) Identification of apolipoprotein n-acyltransferase (LNT) in mycobacteria. J Biol Chem 284: 27146–27156.
7. Pecora ND, Gehring AJ, Canaday DH, Boom WH, Harding CV (2006) *Mycobacterium tuberculosis* LprA is a lipoprotein agonist of TLR2 that regulates innate immunity and APC function. J Immunol 177: 422–429.
8. Krutzik SR, Ochoa MT, Sieling PA, Uematsu S, Ng YW, et al. (2003) Activation and regulation of Toll-like receptors 2 and 1 in human leprosy. Nat Med 9: 525–532.
9. Takeuchi O, Sato S, Horiuchi T, Hoshino K, Takeda K, et al. (2002) Cutting edge: role of Toll-like receptor 1 in mediating immune response to microbial lipoproteins. J Immunol 169: 10–14.
10. Inaba K, Inaba M, Naito M, Steinman RM (1993) Dendritic cell progenitors phagocytose particulates, including bacillus Calmette-Guerin organisms, and sensitize mice to mycobacterial antigens in vivo. J Exp Med 178: 479–488.
11. Makino M, Maeda Y, Mukai T, Kaufmann SH (2006) Impaired maturation and function of dendritic cells by mycobacteria through IL-1beta. Eur J Immunol 36: 1443–1452.
12. Flynn JL, Chan J, Triebold KJ, Dalton DK, Stewart TA, et al. (1993) An essential role for interferon gamma in resistance to *Mycobacterium tuberculosis* infection. J Exp Med 178: 2249–2254.
13. Stenger S, Modlin RL (2002) Control of *Mycobacterium tuberculosis* through mammalian Toll-like receptors. Curr Opin Immunol 14: 452–457.
14. Ganser JL, Kiessler V, Engele M, Wittke F, Rollinghoff M, et al. (2003) Human NKT cells express granulysin and exhibit antimycobacterial activity. J Immunol 170: 3154–3161.
15. Kaufmann SH (1999) Cell-mediated immunity: dealing a direct blow to pathogens. Curr Biol 9: R97–99.
16. Thoma-Uszynski S, Stenger S, Modlin RL (2000) CTL-mediated killing of intracellular *Mycobacterium tuberculosis* is independent of target cell nuclear apoptosis. J Immunol 165: 5773–5779.
17. Makino M, Baba M (1997) A cryopreservation method of human peripheral blood mononuclear cells for efficient production of dendritic cells. Scand J Immunol 45: 618–622.
18. Maeda Y, Mukai T, Spencer J, Makino M (2005) Identification of an immunomodulating agent from *Mycobacterium leprae*. Infect Immun 73: 2744–2750.
19. Levy L, Ji B (2006) The mouse foot-pad technique for cultivation of *Mycobacterium leprae*. Lepr Rev 77: 5–24.
20. McDermott-Lancaster RD, Ito T, Kohsaka K, Guelpa-Lauras CC, Grosset JH (1987) Multiplication of *Mycobacterium leprae* in the nude mouse, and some applications of nude mice to experimental leprosy. Int J Lepr Other Mycobact Dis 55: 889–895.
21. Hashimoto K, Maeda Y, Kimura H, Suzuki K, Masuda A, et al. (2002) *Mycobacterium leprae* infection in monocyte-derived dendritic cells and its influence on antigen-presenting function. Infect Immun 70: 5167–5176.
22. Hendry C, Dionne K, Hedgepeth A, Carroll K, Parrish N (2009) Evaluation of a rapid fluorescent staining method for detection of mycobacteria in clinical specimens. J Clin Microbiol 47: 1206–1208.
23. Truman RW, Krahenbuhl JL (2001) Viable *Mycobacterium leprae* as a research reagent. Int J Lepr Other Mycobact Dis 69: 1–12.
24. Kishida Y, Yoshikawa H, Myoui A (2007) Parthenolide, a natural inhibitor of Nuclear Factor-kappaB, inhibits lung colonization of murine osteosarcoma cells. Clin Cancer Res 13: 59–67.
25. Bastian M, Braun T, Bruns H, Rollinghoff M, Stenger S (2008) Mycobacterial lipopeptides elicit CD4+ CTLs in *Mycobacterium tuberculosis*-infected humans. J Immunol 180: 3436–3446.

26. Murray RA, Siddiqui MR, Mendillo M, Krahenbuhl J, Kaplan G (2007) *Mycobacterium leprae* inhibits dendritic cell activation and maturation. J Immunol 178: 338–344.
27. Cella M, Scheidegger D, Palmer-Lehmann K, Lane P, Lanzavecchia A, et al. (1996) Ligation of CD40 on dendritic cells triggers production of high levels of interleukin-12 and enhances T cell stimulatory capacity: T-T help via APC activation. J Exp Med 184: 747–752.
28. Yamauchi PS, Bleharski JR, Uyemura K, Kim J, Sieling PA, et al. (2000) A role for CD40-CD40 ligand interactions in the generation of type 1 cytokine responses in human leprosy. J Immunol 165: 1506–1512.
29. Sallusto F, Cella M, Danieli C, Lanzavecchia A (1995) Dendritic cells use macropinocytosis and the mannose receptor to concentrate macromolecules in the major histocompatibility complex class II compartment: downregulation by cytokines and bacterial products. J Exp Med 182: 389–400.
30. Tailleux L, Schwartz O, Herrmann JL, Pivert E, Jackson M, et al. (2003) DC-SIGN is the major *Mycobacterium tuberculosis* receptor on human dendritic cells. J Exp Med 197: 121–127.
31. Geijtenbeek TB, Van Vliet SJ, Koppel EA, Sanchez-Hernandez M, Vandenbroucke-Grauls CM, et al. (2003) Mycobacteria target DC-SIGN to suppress dendritic cell function. J Exp Med 197: 7–17.
32. Langrish CL, McKenzie BS, Wilson NJ, de Waal Malefyt R, Kastelein RA, et al. (2004) IL-12 and IL-23: master regulators of innate and adaptive immunity. Immunol Rev 202: 96–105.
33. Pearce EL, Shen H (2007) Generation of CD8 T cell memory is regulated by IL-12. J Immunol 179: 2074–2081.
34. Shibagaki N, Udey MC (2002) Dendritic cells transduced with protein antigens induce cytotoxic lymphocytes and elicit antitumor immunity. J Immunol 168: 2393–2401.
35. Brightbill HD, Libraty DH, Krutzik SR, Yang RB, Belisle JT, et al. (1999) Host defense mechanisms triggered by microbial lipoproteins through toll-like receptors. Science 285: 732–736.
36. Stenger S, Modlin RL (1999) T cell mediated immunity to *Mycobacterium tuberculosis*. Curr Opin Microbiol 2: 89–93.
37. van de Berg PJ, van Leeuwen EM, ten Berge IJ, van Lier R (2008) Cytotoxic human CD4(+) T cells. Curr Opin Immunol 20: 339–343.
38. Canaday DH, Wilkinson RJ, Li Q, Harding CV, Silver RF, et al. (2001) CD4(+) and CD8(+) T cells kill intracellular *Mycobacterium tuberculosis* by a perforin and Fas/Fas ligand-independent mechanism. J Immunol 167: 2734–2742.
39. Ochoa MT, Stenger S, Sieling PA, Thoma-Uszynski S, Sabet S, et al. (2001) T-cell release of granulysin contributes to host defense in leprosy. Nat Med 7: 174–179.
40. Dieli F, Troye-Blomberg M, Ivanyi J, Fournie JJ, Krensky AM, et al. (2001) Granulysin-dependent killing of intracellular and extracellular *Mycobacterium tuberculosis* by Vgamma9/Vdelta2 T lymphocytes. J Infect Dis 184: 1082–1085.
41. Heibein JA, Barry M, Motyka B, Bleackley RC (1999) Granzyme B-induced loss of mitochondrial inner membrane potential (Delta Psi m) and cytochrome c release are caspase independent. J Immunol 163: 4683–4693.
42. Davis JE, Smyth MJ, Trapani JA (2001) Granzyme A and B-deficient killer lymphocytes are defective in eliciting DNA fragmentation but retain potent in vivo anti-tumor capacity. Eur J Immunol 31: 39–47.

JOURNAL OF CLINICAL MICROBIOLOGY, Nov. 2011, p. 3829–3836 Vol. 49, No. 11
0095-1137/11/$12.00 doi:10.1128/JCM.00783-11

Nineteen Cases of Buruli Ulcer Diagnosed in Japan from 1980 to 2010[▽]

Kazue Nakanaga,[1]* Yoshihiko Hoshino,[1] Rie Roselyne Yotsu,[2] Masahiko Makino,[1] and Norihisa Ishii[1]

Leprosy Research Center, National Institute of Infectious Diseases, Tokyo, Japan 189-0002,[1] and Department of Dermatology, National Center for Global Health and Medicine, Tokyo, Japan 162-8655[2]

Received 19 April 2011/Returned for modification 7 June 2011/Accepted 15 August 2011

The etiology, clinical manifestations, and treatment of 19 sporadic cases of Buruli ulcer (BU) in Japan are described. The cases originated in different regions of Honshu Island, with no evidence of patient contact with an aquatic environment. The majority (73.7%) of cases occurred in females, with an average age of 39.1 years for females and 56.8 years for males. All patients developed ulcers on exposed areas of the skin (e.g., face, extremities). Most ulcers were <5 cm in diameter (category I), except in one severe progressive case (category II). Pain was absent in 10 of the 19 cases. Fourteen ulcers were surgically excised, and nine patients needed skin grafting. All cases were treated with various antibiotic regimens, with no reported recurrences as of March 2011. *Mycobacterium ulcerans*-specific IS*2404* was detected in all cases. Ten isolates had identical 16S rRNA gene sequences, which were similar to those of *M. ulcerans*. However, the *rpoB* gene showed a closer resemblance to *Mycobacterium marinum* or *Mycobacterium pseudoshottsii*. PCR identified pMUM001 in all isolates but failed to detect one marker. DNA-DNA hybridization misidentified all isolates as *M. marinum*. The drug susceptibility profile of the isolates also differed from that of *M. ulcerans*. Sequence analysis revealed "*Mycobacterium ulcerans* subsp. *shinshuense*" as the etiologic agent of BU in Japan. Clinical manifestations were comparable to those of *M. ulcerans* but differed as follows: (i) cases were not concentrated in a particular area; (ii) there was no suspected connection to an aquatic environment; (iii) drug susceptibility was different; and (iv) bacteriological features were different.

Buruli ulcer (BU) was first reported in 1935 as a series of unusual painless ulcers in a patient from southeast Australia (2). Thirteen years after the first report, the etiological agent of the ulcer was determined to be *Mycobacterium ulcerans*, a previously unknown mycobacterium (5, 14). During the 1960s, many *M. ulcerans* infections were reported in Uganda, especially in Buruli County, for which this disease was eventually named (3, 32). It is a necrotizing disease of the skin that mostly affects children, producing massive ulcers and permanent, disabling scars. At present, the disease is found primarily in West and Central Africa and in humid tropical areas: BU has been reported in 32 countries, and *M. ulcerans* infection is the third most common mycobacterial infection, after tuberculosis and leprosy. Treatment of progressive cases is difficult and generally requires surgery, usually accompanied by skin grafting and prolonged courses of antibiotics (21, 34).

The first reported case of BU in Japan occurred in 1980 in a 19-year-old woman who had never been abroad (15). The causative agent was isolated and classified as "*Mycobacterium ulcerans* subsp. *shinshuense*" because it was closely related to *M. ulcerans* (31). The disease was not seen again until a 37-year-old woman was affected in 2003 (10). The number of cases increased gradually, until 19 cases had been detected by December 2010 (K. Nakanaga, Y. Hoshino, and N. Ishii, presented at the WHO Annual Meeting on Buruli Ulcer, Geneva, Switzerland, 22 to 24 March 2010). We conducted a comprehensive study using these 19 clinical samples and/or isolated bacteria. Etiology, differential diagnosis, clinical manifestations, and treatments are discussed in this report.

(The preliminary results of this study were presented by K.N. and R. R. Y. in the WHO Annual Meeting on Buruli Ulcer, Geneva, Switzerland, 28 to 30 March 2011.)

MATERIALS AND METHODS

Patients. The research protocol was approved by the institutional review board of the National Institute of Infectious Diseases, Japan. The BU diagnostic criteria were established prior to this study. The primary characteristic was the presence of a clinical lesion, which usually started as a painless subcutaneous nodule, and which secondarily ulcerated with characteristic undermined edges. Other preulcerative forms consisted of papules affecting only the skin, plaques (large, firm, painless, and raised lesions), and edema (a severe form of the disease). Apart from the clinical lesions, at least one of the following criteria must be included for a diagnosis of BU: (i) detection of acid-fast bacilli in a smear from a swab or a biopsy specimen after Ziehl-Neelsen staining, (ii) growth on 7H11 or Ogawa medium, (iii) histopathological confirmation, or (iv) PCR amplification of IS*2404*, an *M. ulcerans*-specific repetitive element. This article is a summary of all BU cases diagnosed to date in Japan. Some have already been published elsewhere as case reports in Japanese and/or English (6, 7, 10, 12, 16, 28, 35).

PCR, sequencing, and phylogenetic analyses. All PCRs targeting IS*2404* (18) were performed on extracted DNA from one or more of the following: fresh skin biopsy specimens, a thin section of formalin-fixed, paraffin-embedded skin, and bacteria isolated from a skin lesion. Briefly, the PCR product, amplified using forward primer PU4F and reverse primer PU7Rbio (Table 1), was electrophoresed on a 2% agarose gel and was stained with ethidium bromide.

The sequences of the internal transcribed spacer between the 16S and 23S rRNA genes (ITS region) and of the 16S rRNA, *rpoB*, and *hsp65* genes were analyzed with the primers listed in Table 1. Amplified PCR products (sizes shown in Table 1) were directly sequenced using the ABI Prism 310 PCR genetic analyzer (Applied Biosystems, Foster City, CA) (16). Sequences were obtained for 1,475- or 1,478-bp (16S rRNA gene), 272-bp (ITS region), 315-bp (*rpoB*), and

* Corresponding author. Mailing address: Department of Mycobacteriology, Leprosy Research Center, National Institute of Infectious Diseases, 4-2-1 Aoba-cho, Higashimurayama-shi, Tokyo 189-0002, Japan. Phone: 81-42-391-8211. Fax: 81-42-394-9092. E-mail: nakanaga@nih.go.jp.

▽ Published ahead of print on 31 August 2011.

TABLE 1. Primer sequences

Primer	Sequence (5′–3′)	PCR target (fragment size [bp])	Reference
PU4F PU7Rbio	GCGCAGATCAACTTCGCGGT GCCCGATTGGTGCTCGGTCA	IS*2404* (154)	18
8F16S 1047R16S	AGAGTTTGATCCTGGCTCAG TGCACACAGGCCACAAGGGA	16S rRNA gene (1,515 or 1,518)	24
830F16S 1542R16S	GTGTGGGTTTCCTTCCTTGG AAGGAGGTGATCCAGCCGCA		
ITSF ITSR	TTGTACACACCGCCCGTC TCTCGATGCCAAGGCATCCACC	16S–23S ITS region (ca. 340)	23
MF MR	CGACCACTTCGGCAACCG TCGATCGGGCACATCCGG	*rpoB* (341)	11
TB11 TB12	ACCAACGATGGTGTGTCCAT CTTGTCGAACCGCATACCCT	*hsp65* (441)	30
RepAF RepAR	CTACGAGCTGGTCAGCAATG ATCGACGCTCGCTACTTCTG	*repA* in pMUM001 (413)	26
ParAF ParAR	GCAAGCTGGGCAATGTTTAT GTCCGGTCCTTGATAGGTCA	*parA* in pMUM001 (501)	26
MUP11F MUP11R	ACCACCCAAGAGTGGAACTG TGTCGTGTCGAGGTATGTGG	Serine/threonine protein kinase in pMUM001 (479)	26
MLSloadF MLSloadR	GGGCAATCGTCCTCACTG CAAGGGCAGTCTTGATTAGG	*mls* load in pMUM001 (560)	26
MLSAT(II)F MLSAT(II)R	AACGTTGAATCCCGTTTTTG GCACCACAAAGGAACGTCTAA	*mlsAT(II)* in pMUM001 (504)	26
TEIIF TEIIR	ATTCAAACGGATGCGAACTG ACATTGCTGGACAAACGACA	Type II thioesterase in pMUM001 (500)	26
MUP045F MUP045R	CAGCAAGTAACGGTGGAACA ACGTGGCCCATTTGTCTTAG	Type III ketosynthase in pMUM001 (496)	26
P450F P450R	CCCACCTCGTCGTTAGTCAT GTGCTCGGTGATCCAGAAGT	P450 in pMUM001 (500)	26

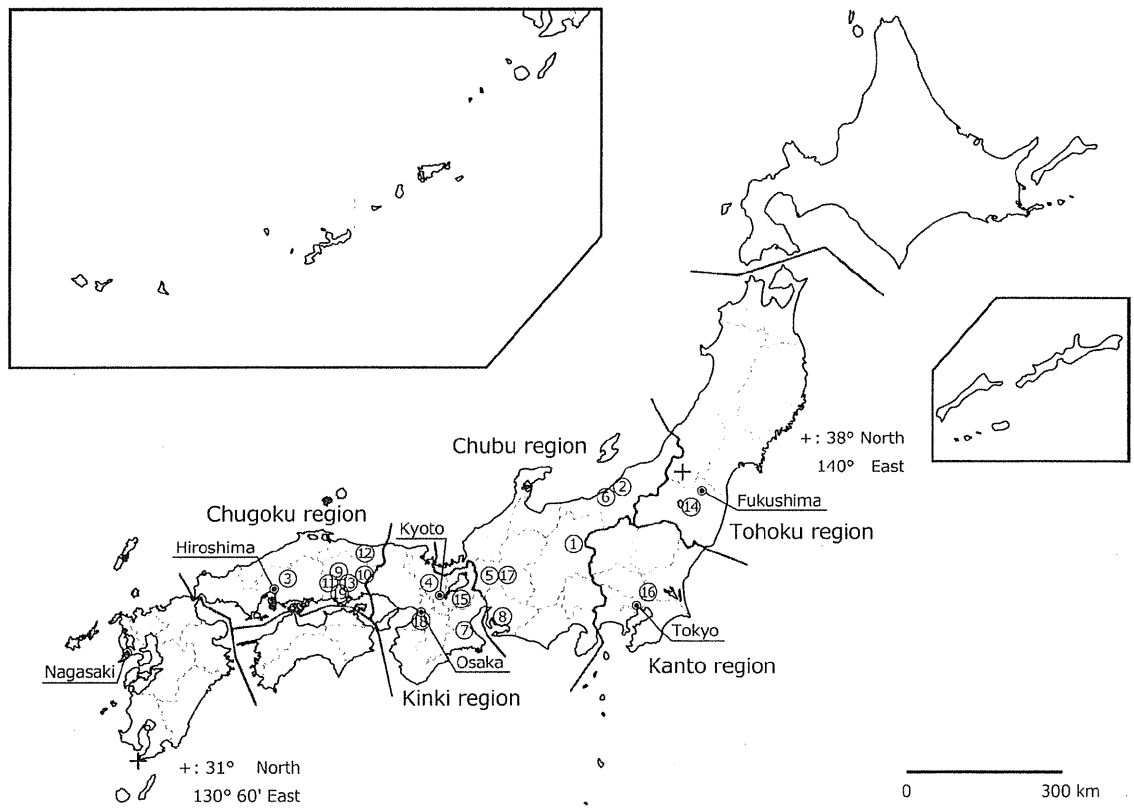

FIG. 1. Distribution of BU patients in Japan. Most of the patients lived in a typical temperate region, and all lived on the island of Honshu. The two plus signs on the map indicate 38°N, 140°E, and 31°N, 130°60′E, placing most of the island in the temperate zone.

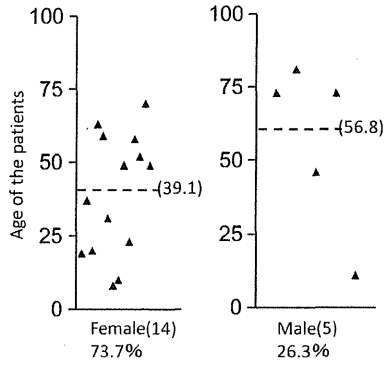

FIG. 2. Ages and genders of BU patients in Japan.

401-bp (*hsp65*) fragments. Ten clinical isolates were compared to six reference strains: *M. ulcerans* ITM 98-912, *M. ulcerans* ATCC 19423^T, *M. ulcerans* Agy99 (25), *Mycobacterium marinum* ATCC 927^T, *M. marinum* clinical isolate LRC 112509, and *Mycobacterium pseudoshottsii* JCM 15466^T. A similarity search was also performed with other mycobacterial reference strains and the 10 clinical strains using the DNA Data Bank of Japan (DDBJ) (8). Phylogenetic analyses were performed using the MEGA software package, version 4.0.2 (build 4028) (29). A tree was constructed using the neighbor-joining method with Kimura's two-parameter distance correction model with 1,000 bootstrap replications.

Finally, primers for eight pMUM001 sequences that encode toxic lipid mycolactone-producing enzymes (26) were used to compare the PCR products of the 10 clinical isolates, *M. ulcerans* ITM 98-912, *M. ulcerans* ATCC 19423^T, *M. ulcerans* Agy99, and *M. pseudoshottsii* JCM 15466^T.

DNA-DNA hybridization assay. A commercially available DNA-DNA hybridization method (DDH Mycobacteria kit; Kyokuto Pharmaceutical Industrial, Tokyo, Japan) was used to identify mycobacterial species isolated from patients (13). The 18 strains in the *Mycobacterium* reference panel included *M. marinum* but not *M. ulcerans*, *M. ulcerans* subsp. *shinshuense*, or *M. pseudoshottsii*.

Growth characteristics and biochemical assay. Culture growth characteristics were determined, and identification was performed, as described previously (16) for 10 of the 11 mycobacterial isolates recovered from patients.

Assay for susceptibility to antimycobacterial drugs. The susceptibilities of the clinical isolates to antibiotics *in vitro* were determined by microdilution (33) using the BrothMIC NTM kit (Kyokuto Pharmaceutical Industrial Co. Ltd., Tokyo, Japan), with modification of the incubation temperature (32°C) and period (2 to 3 weeks). MIC testing was performed in triplicate on different days, with two of three matching MICs used as the criterion for MIC determination.

Nucleotide sequence accession numbers. The DNA sequences of the 16S rRNA (1,475-bp), *hsp65* (401-bp), *rpoB* (315-bp), and ITS (272-bp) fragments from the reference strains (*M. ulcerans* ITM 98-912, *M. ulcerans* ATCC 19423^T, *M. ulcerans* Agy99, *M. marinum* ATCC 927^T, *M. marinum* clinical isolate LRC 112509, and *M. pseudoshottsii* JCM 15466^T) and 10 clinical isolates have been deposited in the International Nucleotide Sequence Database (INSD) through the DDBJ under accession numbers AB548711 to AB548734 and AB624260 to AB624295.

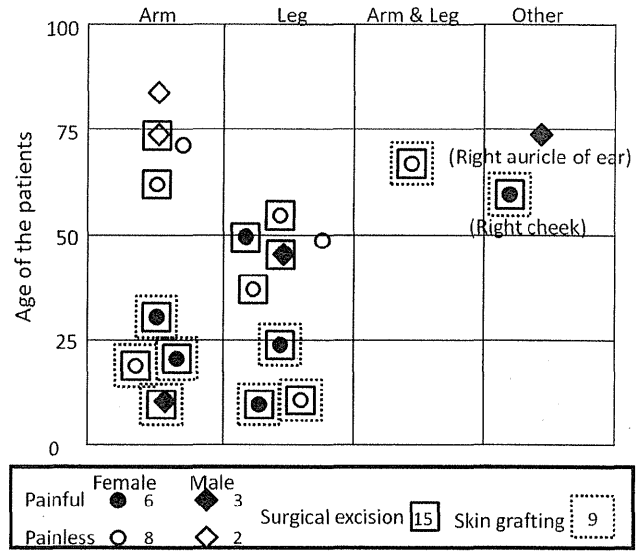

FIG. 4. Localization, pain, and surgical treatment of ulcer lesions by age and gender.

RESULTS

Epidemiology. Nineteen BU cases from Japan have been reported to the WHO BU committee as of December 2010. Many of the *M. ulcerans*-related reports of BU have originated in tropical wetlands. However, Japan is located in eastern Asia, and the majority of the country is covered by mountainous terrain. The 19 cases were distributed between latitudes 34°N and 38°N, in a typical temperate region of Japan.

There was no geographic focal point in the distribution of the BU cases. However, all of the patients lived on Honshu, the largest island of Japan. Seven cases were found in the Chugoku region (western Honshu), 6 in the Chubu region (central Honshu), 4 in the Kinki region (between Chugoku and Chubu), 1 in the Tohoku region (northern Honshu), and 1 in the Kanto region (eastern Honshu) (Fig. 1).

Fourteen (73.7%) subjects were female, and 5 (26.3%) were male. The average age was 39.1 years (range, 8 to 70 years) for the females and 56.8 years (range, 11 to 81 years) for the males (Fig. 2). Despite careful and precise patient interviews, none of the cases could be linked to an aquatic environment.

The affected areas were on exposed sites, such as arms (8

FIG. 3. (A) Buruli ulcer case 8: a category I ulcer on the right forearm. (B) Buruli ulcer case 3: a category II ulcer on the right elbow extensor surface.

TABLE 2. IS*2404* detection in 19 cases of BU in Japan

Case no.	Yr of diagnosis	Origin (region)	Sample type			Isolation period[c]
			Tissue sample[a]	Paraffin section[b]	Isolate	
1	1980	Chubu	NT	NT	P	4 wk
2	2004	Chubu	NT	NT	P	S
3	2006	Chugoku	P	P	P	11 wk
4	2005	Kinki	NT	NT	P	6 wk
5	2007	Chubu	P	P	P	8 wk
6	2007	Chubu	NT	NT	P	S
7	2007	Kinki	NT	NT	P	S
8	2008	Chubu	P	NT	P	11 mo
9	2008	Chugoku	P	NT	NT	NT
10	2009	Chugoku	P	NT	NT	NT
11	2009	Chugoku	P	P	NT	NT
12	2009	Chugoku	P	P	NT	NT
13	2009	Chugoku	NT	P	P	12 wk
14	2009	Tohoku	P	NT	NT	NT
15	2010	Kinki	P	NT	NT	6 wk
16	2010	Kanto	P	P	NT	NT
17	2010	Chubu	P	P	P	5 wk
18	2010	Kinki	P	P	NT	NT
19	2010	Chugoku	P	P	NT	NT

[a] Frozen or fresh skin biopsy sample. NT, not tested; P, positive.
[b] Sliced from a formalin-fixed, paraffin-embedded skin biopsy sample.
[c] S, isolation was successful, but the incubation period was uncertain.

cases), legs (8 cases), the right auricle of the ear (1 case), the right cheek (1 case), and both arms and legs (1 case). While skin ulcer lesions were present in all cases, most were smaller than 5 cm in diameter and were classified as category I (Fig. 3A) (36). In one severe case, the patient presented with a progressive ulcer larger than 10 cm in diameter on the extensor surface of the right elbow, which fell into category II (Fig. 3B). Nine patients (47%) experienced pain, although in many reported cases, BU is painless or only slightly painful (Fig. 4).

Genotypic analysis. PCR screening to detect IS*2404* gave a positive result for at least one of three sample types in all 19 cases. We should note that fresh tissue samples were the source of the template for 13 cases, while formalin-fixed, paraffin-embedded specimens were also used for 9 cases, and all were positive (Table 2). Mycobacteria were successfully isolated in 11 of the 19 cases; however, further bacteriological tests, including genotypic analysis, were performed on 10 available isolates.

The 16S rRNA gene sequences (1,475 bp) of these isolates were identical to each other but partially different from those of *M. ulcerans*, *M. marinum*, and *M. pseudoshottsii* (Table 3). The *hsp65* (401-bp), *rpoB* (315-bp), and internal transcribed spacer (ITS) (272-bp) sequences were also identical among isolates. Sequence analysis identified *M. ulcerans* subsp. *shinshuense* as the bacterium in the clinical samples. Phylogenetic trees based on 16S rRNA and *hsp65* gene sequences showed a close relationship between *M. ulcerans* subsp. *shinshuense* and *M. ulcerans* (Fig. 5A and B). A phylogenetic analysis of the 16S–23S intergenic spacer region showed no differences between *M. ulcerans* subsp. *shinshuense*, *M. marinum*, and *M. ulcerans* and found that *M. pseudoshottsii* is a close relative (Fig. 5C). In contrast, the tree based on the *rpoB* gene showed a closer relationship of *M. ulcerans* subsp. *shinshuense* to *M. marinum* and *M. pseudoshottsii* than to *M. ulcerans*, supporting the premise that *M. ulcerans* subsp. *shinshuense* is distinct from *M. ulcerans* (Fig. 5D).

Next, amplification of eight pMUM001-associated genes was used to determine whether these isolates had genes that encode toxic lipid mycolactone-producing enzymes. All isolates

TABLE 3. Comparison of 16S rRNA gene sequences of 10 *M. ulcerans* subsp. *shinshuense* isolates and related mycobacterial strains

Strain	Country	Nucleotide(s) at the following *Escherichia coli* 16S rRNA gene sequence position(s):								
		95	487–488	492	969	1007	1215	1247	1288	1449–1451[a]
M. ulcerans subsp. *shinshuense*										
ATCC 33728	Japan	T	GG	G	A	G	T	G	G	ACCC---TTTG
JATA753	Japan	T	GG	G	A	G	T	G	G	ACCC---TTTG
0401	Japan	T	GG	G	A	G	T	G	G	ACCC---TTTG
0501	Japan	T	GG	G	A	G	T	G	G	ACCC---TTTG
0701	Japan	T	GG	G	A	G	T	G	G	ACCC---TTTG
0702	Japan	T	GG	G	A	G	T	G	G	ACCC---TTTG
0703	Japan	T	GG	G	A	G	T	G	G	ACCC---TTTG
0801	Japan	T	GG	G	A	G	T	G	G	ACCC---TTTG
0901	Japan	T	GG	G	A	G	T	G	G	ACCC---TTTG
1001	Japan	T	GG	G	A	G	T	G	G	ACCC---TTTG
M. ulcerans										
ITM 98-912	China	T	GG	G	A	G	T	G	G	ACCC---TTTG
ATCC 19423^T	Australia	T	GG	A	A	G	T	G	C	ACCC---TTTG
Agy99	Ghana	T	GG	A	A	G	T	G	C	ACCCTTTTTTG
M. marinum										
ATCC 927^T	United States	T	GG	A	A	G	T	A	A	ACCC---TTTG
112509	Japan	T	GG	A	A	G	T	A	A	ACCC---TTTG
M. pseudoshottsii JCM 15466^T	United States	C	GA	A	G	T	C	A	A	ACCC---TTTG

[a] Hyphens indicate gaps.

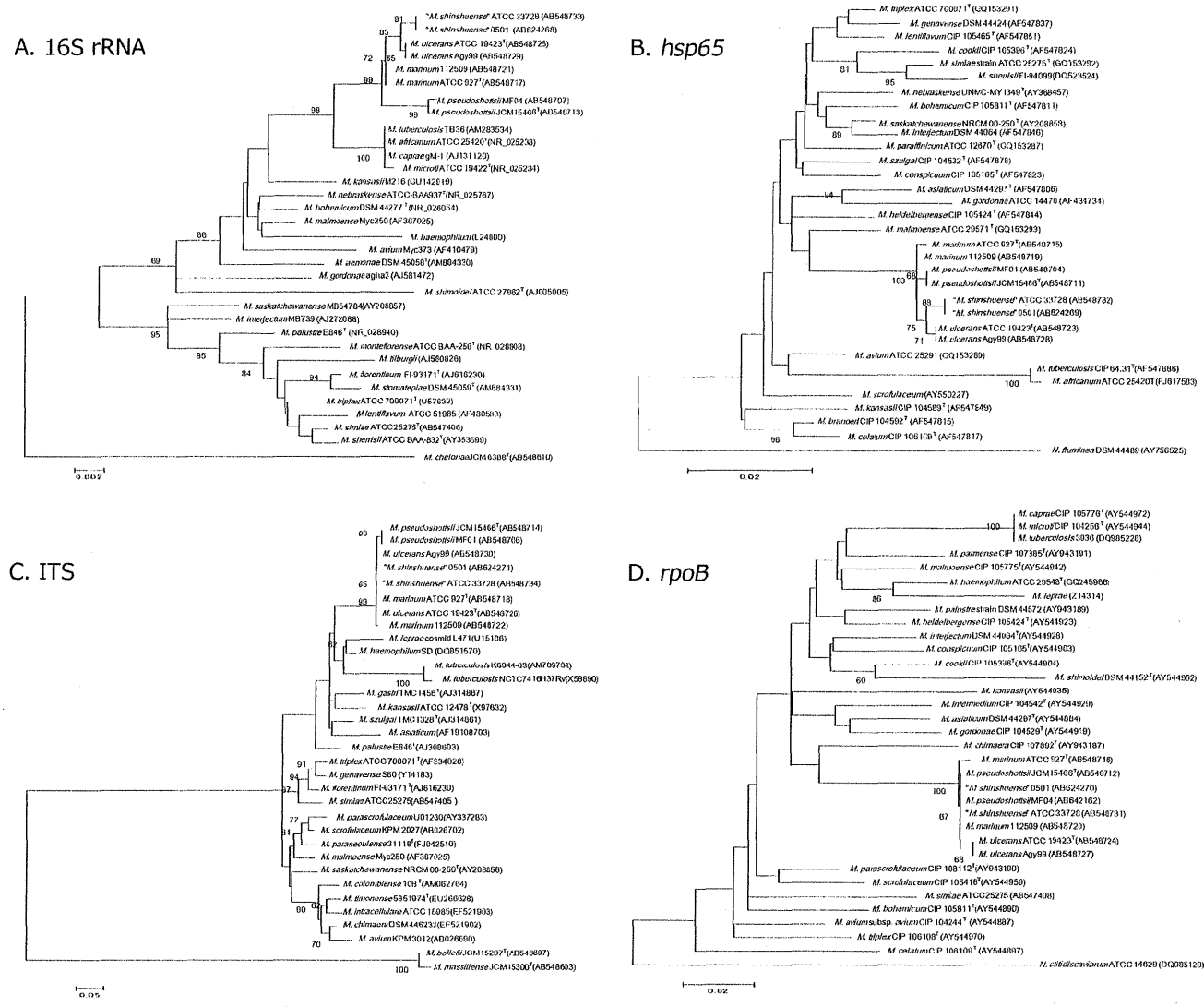

FIG. 5. Phylogenetic analyses of *M. ulcerans* subsp. *shinshuense* based on the 16S rRNA gene (A), the *hsp65* gene (B), the 16S–23S intergenic spacer region (C), and the *rpoB* gene (D).

showed positive results, but as previously reported, the band representing the serine/threonine protein kinase (STPK) gene was absent in *M. ulcerans* subsp. *shinshuense* strains (16). However, this phenomenon was also observed with one strain of *M. ulcerans*, ITM 98-912, that was isolated in China (4). All eight bands were detected in the *M. ulcerans* strains isolated from Australia and Ghana. *M. pseudoshottsii* lacked the band representing P450, but the other seven bands were successfully amplified (Table 4).

A commercially available DNA-DNA hybridization assay was used to verify species identity. The kit contained a reference panel of 18 mycobacterial strains that included *M. marinum* but not *M. ulcerans*, *M. ulcerans* subsp. *shinshuense*, or *M. pseudoshottsii*. All 10 isolates showed clear positive signals for *M. marinum* (Table 5, rightmost column).

Biochemical characteristics. The 10 isolates exhibited the same characteristics: rough colonies and yellow pigmentation, even when grown in the dark. The slowly growing mycobacterium formed visible colonies at 25°C and 32°C on a 2% Ogawa egg slant, but not at 37°C or 42°C. No growth was seen on a medium supplemented with 500 μg/ml *p*-nitrobenzoic acid or 5% NaCl. The isolates were negative for niacin, nitrate reduction, arylsulfatase (3 days), Tween 80 hydrolysis, pyrazinamidase, and iron uptake but were positive for semiquantitative catalase and 68°C catalase and urease. Comparisons between *M. ulcerans* subsp. *shinshuense*, *M. ulcerans*, and *M. marinum* are summarized in Table 5. These results were in accordance with those of a previous report (22) except for the positive result of *M. ulcerans* subsp. *shinshuense* on the urease test.

Drug susceptibility assays. Table 6 shows the results of testing of the susceptibilities of *M. ulcerans* subsp. *shinshuense* ATCC 33728 and *M. ulcerans* subsp. *shinshuense* clinical isolate 0501 to antimicrobial agents. These isolates exhibited high susceptibilities to streptomycin, kanamycin, levofloxacin, and clarithromycin. Notably, *M. ulcerans* subsp. *shinshuense* was more susceptible to streptomycin, kanamycin, and clarithromy-

TABLE 4. PCR detection of eight pMUM001-associated genes in 10 *M. ulcerans* subsp. *shinshuense* isolates and related mycobacterial strains

Strain	Country	Presence or absence of the following pMUM001 marker gene[a]:							
		repA	*parA*	STPK	*mls* (load)	*mlsAT(II)*	TEII	KSIII	P450
M. ulcerans subsp. *shinshuense*									
ATCC 33728	Japan	+	+	−	+	+	+	+	+
JATA753	Japan	+	+	−	+	+	+	+	+
0401	Japan	+	+	−	+	+	+	+	+
0501	Japan	+	+	−	+	+	+	+	+
0701	Japan	+	+	−	+	+	+	+	+
0702	Japan	+	+	−	+	+	+	+	+
0703	Japan	+	+	−	+	+	+	+	+
0801	Japan	+	+	−	+	+	+	+	+
0901	Japan	+	+	−	+	+	+	+	+
1001	Japan	+	+	−	+	+	+	+	+
M. ulcerans									
ITM 98-912	China	+	+	−	+	+	+	+	+
ATCC 19423^T	Australia	+	+	+	+	+	+	+	+
Agy99	Ghana	+	+	+	+	+	+	+	+
M. pseudoshottsii JCM 15466^T	United States	+	+	+	+	+	+	+	−

[a] +, present; −, absent. STPK, serine/threonine protein kinase; TEII, type II thioesterase; KSIII, type III ketosynthase.

cin than the *M. ulcerans* reference strains. Like the *M. ulcerans* reference strains, *M. ulcerans* subsp. *shinshuense* was susceptible to amikacin but resistant to ethambutol, isoniazid, and ethionamide.

Treatment. The 19 patients were treated with various antibiotic regimens. Clarithromycin was effective for many of the Japanese patients (12 cases). Rifampin was successful in the first case and was used thereafter in 9 cases. Attempts at treatment with other medications, alone and in combinations, were also made (Table 7). In 2 cases, the initial choice of antibiotics was ineffective, and they were changed. In 2 other cases, the antibiotic treatment was discontinued due to adverse effects. In addition to antibiotic treatment, 13 patients underwent surgical excision, and 9 needed skin grafting (Fig. 4). No relapses had been reported as of March 2011.

DISCUSSION

This is the first report that comprehensively analyzes both the genotypic and the biochemical profiles of a causative agent of Buruli ulcer in Japan. It is noteworthy that BU in Japan was induced by *Mycobacterium ulcerans* subsp. *shinshuense*, not by *M. ulcerans*. We compared certain characteristics of *M. ulcerans* and *M. ulcerans* subsp. *shinshuense* by several analyses. They are relatively similar; detection of IS*2404* by PCR was the most important test for early diagnosis and differential diag-

TABLE 5. Bacteriological characteristics of 10 *M. ulcerans* subsp. *shinshuense* isolates and closely related mycobacterial strains

Strain	Country	Biochemical characteristic							Identification of *M. marinum*[b]
		Growth rate	Colony morphology	Pigment in dark	Urease activity	Tween 80 hydrolysis	PZase[a] activity	MPB64 production	
M. ulcerans subsp. *shinshuense*									
ATCC 33728	Japan	Low	Rough	Yellow	+	−	−	−	+
JATA753	Japan	Low	Rough	Yellow	+	−	−	−	+
0401	Japan	Low	Rough	Yellow	+	−	−	−	+
0501	Japan	Low	Rough	Yellow	+	−	−	−	+
0701	Japan	Low	Rough	Yellow	+	−	−	−	+
0702	Japan	Low	Rough	Yellow	+	−	−	−	+
0703	Japan	Low	Rough	Yellow	+	−	−	−	+
0801	Japan	Low	Rough	Yellow	+	−	−	−	+
0901	Japan	Low	Rough	Yellow	+	−	−	−	+
1001	Japan	Low	Rough	Yellow	+	−	−	−	+
M. ulcerans									
ITM 98-912	China	Low	Rough	Yellow	+	−	−	−	+
ATCC 19423^T	Australia	Low	Rough	None	−	−	−	−	+
Agy99	Ghana	Low	Rough	Yellow	−	−	−	−	+
M. marinum ATCC 927^T	United States	Medium	Smooth	None	+	+	+	−	+

[a] PZase, pyrazinamidase.
[b] By use of the DDH Mycobacteria kit (Kyokuto Pharmaceutical Industrial, Tokyo, Japan).

TABLE 6. Drug susceptibility test results

Antimycobacterial drug[a]	MIC (μg/ml) for:			
	M. ulcerans subsp. *shinshuense*		*M. ulcerans*	
	ATCC 33728	0501	ATCC 19423^T	Agy99
SM	0.125	0.25	1	4
EB	16	8	16	128
KM	0.25	0.25	1	1
INH	8	8	>32	>32
RFP	0.06	0.06	0.06	0.06
LVFX	0.25	0.5	0.5	8
CAM	0.03	0.06	0.25	0.125
TH	16	8	16	16
AMK	0.5	0.5	0.5	0.5

[a] SM, streptomycin; EB, ethambutol; KM, kanamycin; INH, isoniazid; RFP, rifampin; LVFX, levofloxacin; CAM, clarithromycin; TH, ethionamide; AMK, amikacin.

TABLE 7. Antibiotic treatment regimens for BU cases

Regimen[a]	No. of cases
Single drug	
CAM	2
MINO	1
RFP	1
Two drugs	
CAM, RFP	2
ITZ, MINO	1
LVFX, MINO	1
Three drugs	
CAM, LVFX, RFP	3
CAM, CFPN-PI, NFLX	1
CFPN-PI, LVFX, MINO	1
CAM, MINO, NFLX	1
GRNX, LVFX, MINO	1
Four drugs (EB, LVFX, RFP, SM)	1
Six drugs	
AZM, CAM, CPFX, LVFX, MINO, RFP	1
CAM, EB, GFLX, INH, RFP, SM	1
CAM, CPFX, LVFX, MINO, PZFX, RFP	1

[a] AZM, azithromycin; CAM, clarithromycin; CFPN-PI, cefcapene-pivoxil; CPFX, ciprofloxacin; EB, ethambutol; GFLX, gatifloxacin; GRNX, garenoxacin; INH, isoniazid; ITZ, itraconazole; LVFX, levofloxacin; MINO, minocycline; NFLX, norfloxacin; RFP, rifampin; SM, streptomycin; PZFX, pazufloxacin.

nosis for distinguishing both *M. ulcerans* subsp. *shinshuense* and *M. ulcerans* infections from *M. marinum* infection. Although the DDH Mycobacteria kit could not distinguish *M. ulcerans* and *M. ulcerans* subsp. *shinshuense* from *M. marinum* (Table 5), simultaneous detection of IS*2404* would prevent misidentification. IS*2404* was well amplified from clinical samples and/or isolates in all 19 cases (Table 2). The 16S rRNA gene sequences of *M. ulcerans* subsp. *shinshuense* and *M. ulcerans* are similar, but conserved sites that were different in *M. ulcerans* subsp. *shinshuense* versus *M. ulcerans* were seen (Table 3); these matched perfectly with the sequences reported by Portaels et al. (20) and subsequently found to be useful in discrimination (6, 16). PCR targeting of pMUM001 revealed that all *M. ulcerans* subsp. *shinshuense* isolates lack the band representing the STPK gene, suggesting a small but conservative mutation(s) in *M. ulcerans* subsp. *shinshuense* versus *M. ulcerans* sequences. This PCR test was also applied for detection of a virulent plasmid and for differential diagnosis of *M. ulcerans* versus *M. ulcerans* subsp. *shinshuense* (16). The DNA sequence of the ITS region and the 16S rRNA and *hsp65* genes showed similarity between the *M. ulcerans* subsp. *shinshuense* isolates and *M. ulcerans*. However, the *rpoB* gene showed more similarity to *M. marinum* and *M. pseudoshottsii* than to *M. ulcerans* (Fig. 5). These data were suggestive of the evolutionary paths of these related mycobacterial species (9).

It is noteworthy that *M. ulcerans* subsp. *shinshuense* was identified in all of the isolates from Japanese patients diagnosed with BU. *M. ulcerans* subsp. *shinshuense*, not *M. ulcerans*, could be the primary etiological agent of BU in eastern Asia. It has been reported that the STPK gene was not amplified from the isolate of a BU patient in China (26). While there might be a taxonomical reason, this isolate was finally classified as *M. ulcerans* (4). A more precise genotypic examination might have revealed this to be a case of *M. ulcerans* subsp. *shinshuense* infection. If so, this finding would suggest that *M. ulcerans* subsp. *shinshuense* is distributed not only in Japan, but also in other areas of eastern Asia. Thorough field work and increased vigilance on the part of dermatologists and physicians are needed to determine the predominant cause of BU in eastern Asia. Because disease severity and susceptibility to antibacterial drugs are significantly different for *M. ulcerans* versus *M. ulcerans* subsp. *shinshuense*, they must be identified and distinguished in clinical settings.

The Japanese *M. ulcerans* subsp. *shinshuense* isolates and the Chinese strain of *M. ulcerans* presumably belong to the same cluster, based on genetic analyses such as microarray-based comparative genomic hybridization (9) and comparative sequence analysis of polymorphic variable-number tandem repeats (VNTR) (27). Their genomes were distinctly different from those of *M. ulcerans* strains that originated in other geographic regions. However, one of the VNTR loci can be used to distinguish between the Chinese and Japanese strains (1). Pidot et al. described the clear difference between the two strains by analyzing virulent plasmid genes and the resulting mycolactone production, noting that the Japanese strain produces mycolactone A/B, while the Chinese strain produces a unique mycolactone D (19). Further study is needed to elucidate the evolution and distribution of *M. ulcerans*, and its relation to *M. ulcerans* subsp. *shinshuense*, in Asia.

It is notable that most of the biochemical characteristics (Table 5) and drug susceptibilities (Table 6) of the isolates were the same as those found in a previous report (22), with the exception of the urease test. Interestingly, the Japanese *M. ulcerans* subsp. *shinshuense* isolates, the Chinese strain of *M. ulcerans*, and the related species *M. marinum* were all urease positive, though other strains of *M. ulcerans* originating from Ghana and Australia were urease negative. The urease test is a simple method with clear results that would be useful in distinguishing between *M. ulcerans* and *M. ulcerans* subsp. *shinshuense*.

Clinical manifestation of BU in Japan was essentially similar to that of BU in other countries, but distinct differences in management were observed. Ulcerated areas were usually smaller for Japanese (Fig. 3) than for African patients; how-

ever, the Japanese patients received both surgery and a large array of antimycobacterial drugs (Table 7). In addition, in Africa, most patients who had lesions with cross-sectional diameters of ≤10 cm showed excellent healing without surgery (17). Although the *in vitro* susceptibilities of the Japanese isolates to streptomycin, kanamycin, and clarithromycin are higher than those of the *M. ulcerans* strains from West Africa (Table 6), treatment has been fairly aggressive in Japan. It is speculated that because the majority of doctors and patients in Japan have not experienced and cannot recognize Buruli ulcer disease, they might fear the progression and recurrence of disease. Especially when patients complain of pain (9 patients in this study [47%] experienced pain [Fig. 4]), their doctors and family members are willing to initiate aggressive treatment, even in the absence of an immunodeficiency risk factor. Public information campaigns about the disease are needed, as is the establishment of guidelines for the treatment of Buruli ulcer in Japan. Clarification of the mode of transmission is also important. However, the occurrence of cases has been very sporadic, and none could be linked to an aquatic environment. Thus, the source and route of the infection remain unclear.

ACKNOWLEDGMENTS

This work was supported in part by a Grant-in-Aid for Research on Emerging and Re-emerging Infectious Diseases from the Ministry of Health, Labor, and Welfare of Japan (to Y.H., M.M., and N.I.), by a Grant-in-Aid for Scientific Research (C) from the Ministry of Education, Culture, Sports, Science and Technology of Japan (to Y.H.), and by a Grant-in-Aid for Scientific Research (C) from the Japan Society for the Promotion of Science (to K.N.).

REFERENCES

1. **Ablordey, A., et al.** 2005. Comparative nucleotide sequence analysis of polymorphic variable number tandem repeat loci in *Mycobacterium ulcerans*. J. Clin. Microbiol. **43**:5281–5284.
2. **Alsop, D. G.** 1972. The Bairnsdale ulcer. Aust. N. Z. J. Surg. **41**:317–319.
3. **Clancey, J. K., O. G. Dodge, H. F. Lunn, and M. L. Oduori.** 1961. Mycobacterial skin ulcers in Uganda. Lancet **ii**:951–954.
4. **Faber, W. R., et al.** 2000. First reported case of *Mycobacterium ulcerans* infection in a patient from China. Trans. R. Soc. Trop. Med. Hyg. **94**:277–279.
5. **Fenner, F.** 1951. The significance of the incubation period in infectious diseases. Med. J. Aust. **2**:813–818.
6. **Funakoshi, T., et al.** 2009. Intractable ulcer caused by *Mycobacterium shinshuense*: successful identification of mycobacterium strain by 16S ribosomal RNA 3′-end sequencing. Clin. Exp. Dermatol. **34**:e712–e715.
7. **Imada, H., et al.** 2008. Cutaneous ulcer of a right olecranon due to *Mycobacterium shinshuense*; a case report. Seikeigeka **59**:1440–1445. (In Japanese.)
8. **Kaminuma, E., et al.** 2010. DDBJ launches a new archive database with analytical tools for next-generation sequence data. Nucleic Acids Res. **38**(Database issue):D33–D38.
9. **Käser, M., et al.** 2007. Evolution of two distinct phylogenetic lineages of the emerging human pathogen *Mycobacterium ulcerans*. BMC Evol. Biol. **7**:177.
10. **Kazumi, Y., et al.** 2004. *Mycobacterium shinshuense* isolated from cutaneous ulcer lesion of right lower extremity in a 37-year-old woman. Kekkaku **79**:437–441. (In Japanese.)
11. **Kim, B.-J., et al.** 1999. Identification of mycobacterial species by comparative sequence analysis of the RNA polymerase gene (*rpoB*). J. Clin. Microbiol. **37**:1714–1720.
12. **Kondo, M., et al.** 2009. Leg ulcer caused by *Mycobacterium ulcerans* ssp. *shinshuense* infection. Int. J. Dermatol. **48**:1330–1333.
13. **Kusunoki, S., et al.** 1991. Application of colorimetric microdilution plate hybridization for rapid genetic identification of 22 *Mycobacterium* species. J. Clin. Microbiol. **29**:1596–1603.
14. **MacCallum, P., J. C. Tolhurst, G. Buckle, and H. I. Sissons.** 1948. A new mycobacterial infection in man. I. Clinical aspects. II. Experimental investigations in laboratory animals. III. Pathology of the experimental lesions in the rat. IV. Cultivation of the new mycobacterium. J. Pathol. Bacteriol. **60**:93–122.
15. **Mikoshiba, H., et al.** 1982. A case of atypical mycobacteriosis due to *Mycobacterium ulcerans*-like organism. Nihon Hifukagakkaizassi **92**:557–565. (In Japanese.)
16. **Nakanaga, K., et al.** 2007. "*Mycobacterium ulcerans* subsp. *shinshuense*" isolated from a skin ulcer lesion: identification based on 16S rRNA gene sequencing. J. Clin. Microbiol. **45**:3840–3843.
17. **Nienhuis, W. A., et al.** 2010. Antimicrobial treatment for early, limited *Mycobacterium ulcerans* infection: a randomized controlled trial. Lancet **375**: 664–672.
18. **Phillips, R. C., et al.** 2005. Sensitivity of PCR targeting the IS*2404* insertion sequence of *Mycobacterium ulcerans* in an assay using punch biopsy specimens for diagnosis of Buruli ulcer. J. Clin. Microbiol. **43**:3650–3656.
19. **Pidot, S. J., et al.** 2008. Deciphering the genetic basis for polyketide variation among mycobacteria producing mycolactones. BMC Genomics **9**:462.
20. **Portaels, F., et al.** 1996. Variability in 3′ end of 16S rRNA sequence of *Mycobacterium ulcerans* is related to geographic origin of isolates. J. Clin. Microbiol. **34**:962–965.
21. **Portaels, F., M. T. Silva, and W. M. Meyers.** 2009. Buruli ulcer. Clin. Dermatol. **27**:291–305.
22. **Portaels, F., P. Johnson, and W. M. Meyers (ed.).** April 2001. Buruli ulcer: diagnosis of *Mycobacterium ulcerans* disease. A manual for health care providers. World Health Organization, Geneva, Switzerland. http://whqlibdoc.who.int/hq/2001/WHO_CDS_CPE_GBUI_2001.4.pdf.
23. **Roth, A., et al.** 1998. Differentiation of phylogenetically related slowly growing mycobacteria based on 16S–23S rRNA gene internal transcribed spacer sequences. J. Clin. Microbiol. **36**:139–147.
24. **Springer, B., et al.** 1996. Isolation and characterization of a unique group of slowly growing mycobacteria: description of *Mycobacterium lentiflavum* sp. nov. J. Clin. Microbiol. **34**:1100–1107.
25. **Stinear, T. P., et al.** 2004. Giant plasmid-encoded polyketide synthases produce the macrolide toxin of *Mycobacterium ulcerans*. Proc. Natl. Acad. Sci. U. S. A. **101**:1345–1349.
26. **Stinear, T. P., et al.** 2005. Common evolutionary origin for the unstable virulence plasmid pMUM found in geographically diverse strains of *Mycobacterium* ulcerans. J. Bacteriol. **187**:1668–1676.
27. **Stragier, P., A. Ablordey, L. Durnez, and F. Portaels.** 2007. VNTR analysis differentiates *Mycobacterium ulcerans* and IS*2404* positive mycobacteria. Syst. Appl. Microbiol. **30**:525–530.
28. **Suzuki, S., et al.** 2008. Skin ulcer caused by '*Mycobacterium ulcerans* subsp. *shinshuense* ' infection. Hifubyou Shinryo **30**:145–148. (In Japanese.)
29. **Tamura, K., J. Dudley, M. Nei, and S. Kumar.** 2007. MEGA4: molecular evolutionary genetic analysis (MEGA) software version 4.0. Mol. Biol. Evol. **24**:1596–1599.
30. **Telenti, A., et al.** 1993. Rapid identification of mycobacteria to the species level by polymerase chain reaction and restriction enzyme analysis. J. Clin. Microbiol. **31**:175–178.
31. **Tsukamura, M., and H. Mikoshiba.** 1989. A taxonomic study on a mycobacterium which caused skin ulcer in a Japanese girl and resembled *Mycobacterium ulcerans*. Kekkaku **64**:691–697. (In Japanese.)
32. **Uganda Buruli Group.** 1971. Epidemiology of *Mycobacterium ulcerans* infection (Buruli ulcer) at Kinyara, Uganda. Trans. R. Soc. Trop. Med. Hyg. **65**:763–775.
33. **Wallace, R. J., Jr, D. R. Nash, L. C. Steele, and V. Steingrube.** 1986. Susceptibility testing of slowly growing mycobacteria by a microdilution MIC method with 7H9 broth. J. Clin. Microbiol. **24**:976–981.
34. **Walsh, D. S., F. Portaels, and W. M. Meyers.** 2011. Buruli ulcer: advances in understanding *Mycobacterium ulcerans* infection. Dermatol. Clin. **29**:1–8.
35. **Watanabe, T., et al.** 2010. Buruli ulcer caused by "*Mycobacterium ulcerans* subsp. *shinshuense*." Eur. J. Dermatol. **20**:809–810.
36. **World Health Organization.** October 2004. Provisional guidance on the role of specific antibiotics in the management of *Mycobacterium ulcerans* disease (Buruli ulcer). World Health Organization, Geneva, Switzerland. http://whqlibdoc.who.int/hq/2004/WHO_CD5_CPE_GBUI_2004.10.pdf..

JOURNAL OF BACTERIOLOGY, Oct. 2011, p. 5766–5774 Vol. 193, No. 20
0021-9193/11/$12.00 doi:10.1128/JB.05412-11

Structure and Host Recognition of Serotype 13 Glycopeptidolipid from *Mycobacterium intracellulare*▽†

Takashi Naka,[1,2]‡ Noboru Nakata,[3]‡ Shinji Maeda,[4]‡ Reina Yamamoto,[1,5] Matsumi Doe,[6] Seiko Mizuno,[1,5] Mamiko Niki,[1] Kazuo Kobayashi,[7] Hisashi Ogura,[1,8] Masahiko Makino,[3] and Nagatoshi Fujiwara[1]*

Departments of Bacteriology[1] and Virology,[8] Osaka City University Graduate School of Medicine, Osaka 545-8585, Japan; MBR Co. Ltd., Osaka 560-8552, Japan[2]; Department of Mycobacteriology, Leprosy Research Center, National Institute of Infectious Diseases, Tokyo 189-0002, Japan[3]; Molecular Epidemiology Division, Mycobacterium Reference Center, The Research Institute of Tuberculosis, Japan Anti-Tuberculosis Association, Tokyo 204-8533, Japan[4]; Department of Development Nourishment, Faculty of Human Development, Soai University, Osaka 559-0003, Japan[5]; Department of Chemistry, Graduate School of Science, Osaka City University, Osaka 558-8585, Japan[6]; and Department of Immunology, National Institute of Infectious Diseases, Tokyo 162-8640, Japan[7]

Received 31 May 2011/Accepted 31 July 2011

The *Mycobacterium avium-M. intracellulare* complex (MAIC) is divided into 28 serotypes by a species-specific glycopeptidolipid (GPL). Previously, we clarified the structures of serotype 7 GPL and two methyltransferase genes (*orfA* and *orfB*) in serotype 12 GPL. This study elucidated the chemical structure, biosynthesis gene, and host innate immune response of serotype 13 GPL. The oligosaccharide (OSE) structure of serotype 13 GPL was determined to be 4-2′-hydroxypropanoyl-amido-4,6-dideoxy-β-hexose-(1→3)-4-*O*-methyl-α-L-rhamnose-(1→3)-α-L-rhamnose-(1→3)-α-L-rhamnose-(1→2)-α-L-6-deoxy-talose by using chromatography, mass spectrometry, and nuclear magnetic resonance (NMR) analyses. The structure of the serotype 13 GPL was different from those of serotype 7 and 12 GPLs only in *O*-methylations. We found a relationship between the structure and biosynthesis gene cluster. *M. intracellulare* serotypes 12 and 13 have a 1.95-kb *orfA-orfB* gene responsible for 3-*O*-methylation at the terminal hexose, *orfB*, and 4-*O*-methylation at the rhamnose next to the terminal hexose, *orfA*. The serotype 13 *orfB* had a nonfunctional one-base missense mutation that modifies serotype 12 GPL to serotype 13 GPL. Moreover, the native serotype 13 GPL was multiacetylated and recognized via Toll-like receptor 2. The findings presented here imply that serotypes 7, 12, and 13 are phylogenetically related and confirm that acetylation of the GPL is necessary for host recognition. This study will promote better understanding of the structure-function relationships of GPLs and may open a new avenue for the prevention of MAIC infections.

The increase of drug-resistant mycobacteria and the number of immunocompromised hosts including the HIV epidemic are important problems. The *Mycobacterium avium-M. intracellulare* complex (MAIC) is distributed ubiquitously in the environment and is the most common isolate of nontuberculous mycobacteria, which are now one of the most important environmental pathogen-disseminated infectious agents in both immunocompromised and immunocompetent hosts (26, 31, 39).

The most characteristic feature of mycobacteria is richness in lipids. These hydrophobic cell wall components contribute to the surface properties and are considered to play important roles in their pathogenesis through the host immune responses (8, 17). MAIC expresses a glycopeptidolipid (GPL) as one of the representative lipid components. Structurally, the GPL is composed of two parts, a common tetrapeptido-amino alcohol core and a serotype-specific oligosaccharide (OSE) elongated from 6-deoxy-talose (6-d-Tal). D-Phenylalanine-D-*allo*-threonine-D-alanine-L-alaninol (D-Phe-D-*allo*-Thr-D-Ala-L-alaninol), which is modified with an amido-linked 3-hydroxy or 3-methoxy C_{26}-C_{34} fatty acid at the *N* terminus of D-Phe, and D-*allo*-Thr and terminal L-alaninol are further linked to a 6-d-Tal and 3,4-di-*O*-methyl rhamnose (3,4-di-*O*-Me-Rha), respectively. This portion is called the serotype-nonspecific GPL (apolar GPL). Serotype-specific GPLs (polar GPLs) are produced by extending individual OSE residues from the 6-d-Tal. MAIC species are divided into 28 serotypes by serological reaction and distinctive patterns of polar GPLs on thin-layer chromatography (TLC) (7, 38). The GPL is considered to play crucial roles in the physiology of the bacteria and the host responses to MAIC infection. Several biological and immunological functions of GPLs have been reported (9, 34), but the roles of GPLs are not fully elucidated. Recently, several genes involved in GPL biosynthesis have been characterized (10, 29). To better understand the biological functions and significance of GPLs, we need to clarify the structure and biosynthetic pathways of GPLs.

The chemical structures of only 16 GPLs have been defined (9). Recently, we determined the structures of the serotype 7 and 16 GPLs and identified the gene clusters completing the OSE biosynthesis (13, 14). In addition, two methyltransferase genes of serotype 7- and 12-specific GPL biosynthesis were

* Corresponding author. Mailing address: Department of Bacteriology, Osaka City University Graduate School of Medicine, 1-4-3 Asahimachi, Abeno-ku, Osaka 545-8585, Japan. Phone: 81 6 6645 3746. Fax: 81 6 6645 3747. E-mail: fujiwara@med.osaka-cu.ac.jp.

† Supplemental material for this article may be found at http://jb.asm.org/.

‡ These authors contributed equally to this work.

▽ Published ahead of print on 19 August 2011.

characterized (30). In this process, we found that the structure of the serotype 13 GPL is close to that of the serotype 7 and 12 GPLs. In epidemiological serotyping, Tsang et al. (37) showed that clinical isolates of serotypes 7, 12, and 13 were found in around 10% of non-AIDS patients. However, it was difficult to distinguish serotypes 7, 12, and 13 by only serological and chromatographic techniques because of their structural similarity. The phylogeny of some MAIC strains based on GPL biosynthesis genes has been reported (23). In this study, the complete structure of the serotype 13 GPL was determined, and the genetic relationship between the serotype 7, 12, and 13 GPL biosynthesis was clarified. Moreover, the host innate immune recognition of antigenic serotype 13 GPL and the importance of structural modification were shown. We discuss the phylogeny of MAIC strains on the basis of these GPL biosynthesis genes and the relationship between GPL structure and immunogenicity.

MATERIALS AND METHODS

Bacterial strains and preparation of GPL. *M. intracellulare* serotype 13 (ATCC 35769, ATCC 25122), serotype 7 (ATCC 35847), and serotype 12 (ATCC 35762) strains were purchased from the American Type Culture Collection (Manassas, VA). The GPL preparation was performed as described previously (14, 18). Each strain of *M. intracellulare* was grown on Middlebrook 7H11 agar (Difco Laboratories, Detroit, MI) with 0.5% glycerol and 10% Middlebrook oleic acid-albumin-dextrose-catalase (OADC) enrichment (Difco) at 37°C for 2 to 3 weeks. The heat-killed bacteria were sonicated, and crude lipids were extracted with chloroform-methanol (2:1 [vol/vol]). The crude lipids were hydrolyzed with 0.2 N sodium hydroxide in methanol at 37°C for 2 h, followed by neutralization with 6 N hydrochloric acid. Alkaline-stable lipids were partitioned by a two-layer system with chloroform-methanol (2:1 [vol/vol]) and water. The organic phase was evaporated and precipitated with acetone to remove any acetone-insoluble components. The supernatant was washed (chloroform-methanol, 95:5 [vol/vol]) and eluted (chloroform-methanol, 1:1 [vol/vol]) with a Sep-Pak silica cartridge (Waters Corporation, Milford, MA) for partial purification. The GPL was completely purified by preparative TLC of Silicagel G (Uniplate; 20 by 20 cm, 250 μm; Analtech, Inc., Newark, DE). The TLC plate was developed with chloroform-methanol-water (65:25:4 and 60:16:2 [vol/vol/vol]), until a single spot was obtained. The TLC plate was sprayed with 20% sulfuric acid in ethanol and was charred at 180°C for 3 min. The GPL was detected as a brownish-yellow spot. To recover the GPL, the TLC plate was exposed to iodine vapor, and the GPL spot was marked. The silica gels of the GPL spot were scraped off, and the GPL was eluted with chloroform-methanol (2:1 [vol/vol]). The native GPL was purified by the same method as the alkaline-stable GPL, omitting the hydrolysis with 0.2 N sodium hydroxide.

Preparation of OSE moiety. β-Elimination of the GPL was performed with alkaline borohydride, and the OSE elongated from D-*allo*-Thr was released (14, 18). The GPL was stirred in a solution of equal volumes of ethanol and 10 mg/ml sodium borodeuteride in 0.5 N sodium hydroxide at 60°C for 16 h. The reaction mixture was decationized with Dowex 50W X8 beads (Dow Chemical Company, Midland, MI) and evaporated under nitrogen to remove boric acid. After partition into two layers of chloroform-methanol (2:1 [vol/vol]) and water, the upper aqueous phase was recovered and evaporated, and the OSE was purified as an oligoglycosyl alditol.

MALDI-TOF MS and MALDI-TOF MS/MS. The molecular species of the intact GPL was determined by the matrix-assisted laser desorption ionization–time of flight mass spectrometry (MALDI-TOF MS) with an Ultraflex II (Bruker Daltonics, Billerica, MA). One microgram of the GPL-dissolved chloroform-methanol (2:1 [vol/vol]) was applied to the target plate, and 1 μl of 10 mg/ml 2,5-dihydroxybenzoic acid in chloroform-methanol (1:1 [vol/vol]) was added as a matrix. The intact GPL was analyzed in the Reflectron mode with an accelerating voltage operating in positive mode at 20 kV (4). Then, the fragment pattern of the OSE was analyzed with the MALDI-TOF MS/MS mode. The OSE and 10 mg/ml 2,5-dihydroxybenzoic acid was dissolved in ethanol-water (3:7 [vol/vol]) and applied to the target plate according to the method for intact GPL.

GC/MS of carbohydrates. To determine the glycosyl composition and linkage position, gas chromatography/mass spectrometry (GC/MS) of partially methylated alditol acetate derivatives was performed. Perdeuteromethylation was conducted by the modified procedure of Hakomori (14, 15). The OSE was dissolved with a mixture of dimethyl sulfoxide and sodium hydroxide, followed by the addition of deuteromethyl iodide. After stirring at room temperature for 15 min, the reaction mixture was separated by a two-layer system of water and chloroform. The chloroform-containing perdeuteromethylated OSE layer was collected, washed with water two times, and evaporated completely. Partially deuteromethylated alditol acetate derivatives were prepared from perdeuteromethylated OSE by hydrolysis with 2 N trifluoroacetic acid at 120°C for 2 h, reduction with 10 mg/ml sodium borodeuteride at 25°C for 2 h, and acetylation with acetic anhydride at 100°C for 1 h (14, 19). GC/MS was performed using a benchtop ion trap mass spectrometer (GCMS-QP2010 Plus; Shimadzu Corp., Kyoto, Japan) equipped with a fused capillary column (SP-2380 and Equity-1; 30 m, 0.25-mm inner diameter [ID]; Supelco, Bellefonte, PA). Helium was used

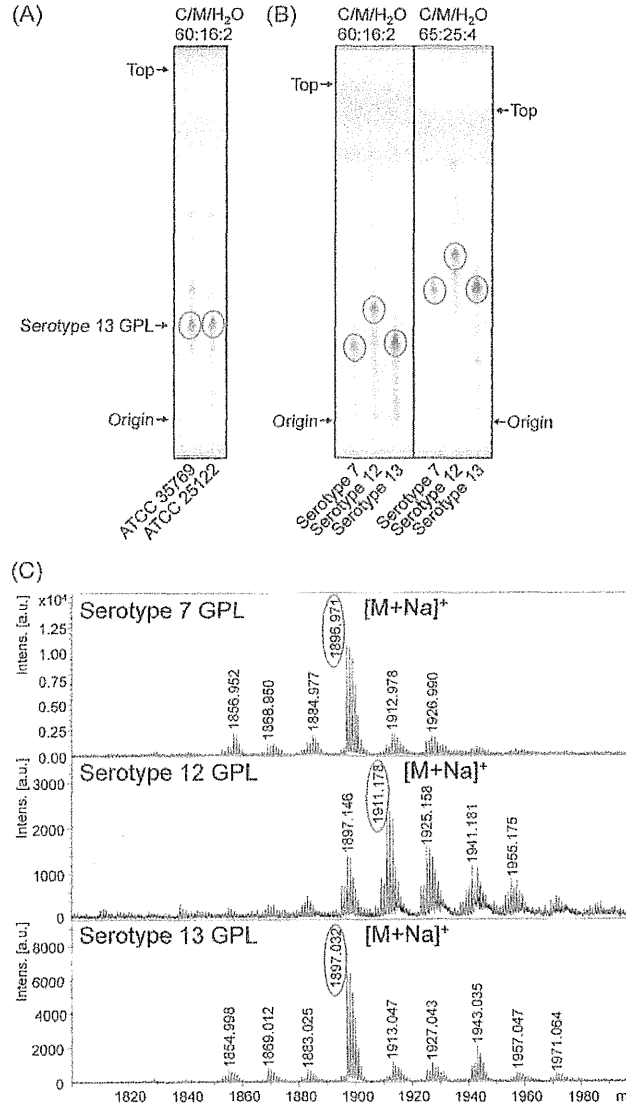

FIG. 1. TLC patterns and MALDI-TOF MS spectra of serotype 7, 12, and 13 GPLs. (A and B) The alkaline-stable lipids derived from *M. intracellulare* serotype 13 ATCC 35769 and ATCC 25122 (A) and the purified serotype 7, 12, and 13 GPLs (B) were developed on TLC plates with solvent systems of chloroform-methanol-water (60:16:2 and 65:25:4 [vol/vol/vol]). (C) The MALDI-TOF MS spectra of serotype 7, 12, and 13 GPLs were acquired using 10 mg/ml 2,5-dihydroxybenzoic acid in chloroform-methanol (1:1 [vol/vol]) as a matrix, and the molecular ions were detected as $[M+Na]^+$ in positive mode. Intens., intensity; a.u., arbitrary units.

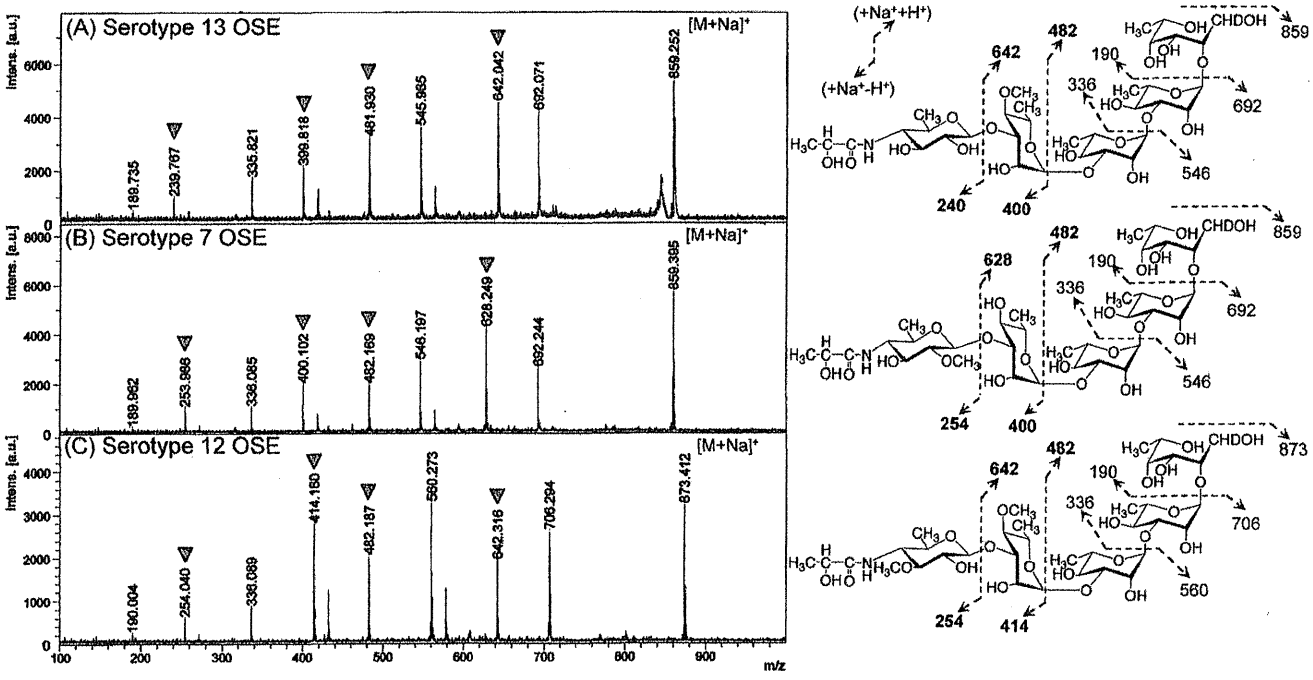

FIG. 2. MALDI-TOF MS/MS spectra of serotype 13, 7, and 12 OSEs (A, B, and C, respectively). The fragment ions by each glycosyl cleavage were detected, and the assigned fragment patterns are illustrated. Arrowheads indicate the characteristic mass numbers of the serotype 13, 7, and 12 OSEs. The matrix was 10 mg/ml 2,5-dihydroxybenzoic acid in ethanol-water (3:7 [vol/vol]), and it was performed in the MS/MS mode. Intens., intensity; a.u., arbitrary units.

as the carrier gas, and the flow rate was 1 ml/min. The temperature program for alditol acetate derivatives was started at 60°C, increased 40°C/min to 220°C, and held for 15 min, followed by an increase of 10°C/min to 260°C and holding for 10 min. The molecular separator and ion source energies were 70 eV, and the accelerating voltage was 8 kV.

NMR of GPL. The OSE was dissolved in deuterium oxide. To define the anomeric configurations of each glycosyl residue, ^{1}H and ^{13}C nuclear magnetic resonance (NMR) was employed. Both homonuclear correlation spectrometry (COSY) and ^{1}H-detected [^{1}H, ^{13}C] heteronuclear multiple-quantum correlation (HMQC) were recorded with a Bruker AVANCE-600 (Bruker BioSpin Corp. Billerica, MA), as described previously (14, 18). Ten microliters of acetone was added to the sample, and its chemical shift values, 2.04 ppm (proton) and 29.8 ppm (carbon), were used as internal controls.

Sequencing of *orfA-orfB* region of *M. intracellulare* serotype 13. PCR was used to amplify the *orfA-orfB* region (30) of *M. intracellulare* serotype 13 (ATCC 35769 and ATCC 25122), using primers *orfA*-F (5′-GCGGATCCAGTGTGCAGACG AGCGGAACT-3′), *orfA*-R (5′-GCGAATTCTTATCGAGAAAAAATAAAA G-3′), *orfB*-F (5′-GCGGATCCACTGCTAGACT CCGCCACCAT-3′), and *orfB*-R (5′-GCGAATTCCTACACCTTCACGGCGAGTC-3′). The amplified fragment was sequenced using a BigDye Terminator cycle sequencing kit, version 3.1 (Applied Biosystems, Foster City, CA), and a sequence analyzer (ABI3130xl; Applied Biosystems).

Transformation of *M. intracellulare* serotype 13 strain with serotype 12 *orfB*. The *orfB* fragments from serotype 12 (sero12-*orfB*) and serotype 13 (sero13-*orfB*) strains were amplified and cloned into pVV16, an expression plasmid vector for mycobacteria, downstream of the hsp60 promoter. *M. intracellulare* serotype 13 ATCC 35769 was transformed with pVV16-sero12-*orfB* and pVV16-sero13-*orfB* by electroporation, and hygromycin- and kanamycin-resistant colonies were isolated. Alkaline-stable lipids were prepared from heat-killed bacteria, and productive GPLs were identified by TLC, MALDI-TOF MS, MALDI-TOF MS/MS, and GC/MS.

Host recognition of native and alkaline-treated serotype 13 GPLs. The host recognition of GPLs was estimated by activations of HEK-blue-2 and -4 cells (InvivoGen, San Diego, CA). HEK-blue-2 and -4 cells are HEK293 cells stably transfected with multiple genes for recognition of Toll-like receptor 2 (TLR2) and TLR4 (including the coreceptors MD2 and CD14). In addition, HEK-blue-2 and -4 cells stably express an optimized alkaline phosphatase gene engineered to be secreted (sAP) and placed under the control of a promoter inducible by several transcription factors, such as NF-κB and alkaline phosphatase-1. HEK-blue-2 and -4 cells were seeded at a concentration of 2×10^5 cells/ml in 96-well flat-bottom tissue culture plates and incubated with Dulbecco's modified Eagle's medium (DMEM) containing 10% fetal bovine serum (FBS) at 37°C in an atmosphere of 5% CO_2 for 3 days. The adherent HEK-blue-2 and -4 cells were stimulated by native and alkaline-treated serotype 13 GPLs. After 24 h of incubation, NF-κB activation was assayed by the levels of sAP in the supernatant. The sAP was measured in duplicate using QUANTI-Blue (InvivoGen) according to the manufacturer's instructions. As positive controls, we used lipopolysaccharide (LPS) from *Escherichia coli* 055:B5 (Sigma-Aldrich, St. Louis, MO) for TLR4 and Pam3CSK4 (InvivoGen) for TLR2. Two independent experiments were performed.

Nucleotide sequence accession number. The nucleotide sequence reported here has been deposited in the NCBI GenBank database under accession number AB557690.

RESULTS

Purification and molecular weight of intact GPL. The serotype 13 GPLs from *M. intracellulare* ATCC 35769 and 25122 were detected as spots on TLC plates and showed the same R_f value (Fig. 1A). Because serotype 13 GPL was predicted to be very close structurally to the serotype 7 and 12 GPLs, the R_f values were compared on TLC plates developed with two different chloroform-methanol-water solvent systems (65:25:4 and 60:16:2 [vol/vol/vol]), respectively. Interestingly, the R_f value of the serotype 13 GPL was lower than that of the serotype 12 GPL and almost the same as that of the serotype 7 GPL in both developing systems (Fig. 1B). The intact molecular weight of each GPL was determined. The MALDI-TOF MS spectrum of the serotype 13 GPL showed *m/z* 1,897 for $[M+Na]^+$ as the main molecular ion in positive mode (Fig.

1C). This mass number is identical to that of the serotype 7 GPL ($[M+Na]^+$: 1,897) and 14 atomic mass units lower than that of the serotype 12 GPL ($[M+Na]^+$: 1,911).

Glycosyl sequence of serotype 13 OSE. To determine the glycosyl sequence of the OSE, MALDI-TOF MS/MS of the oligoglycosyl alditol from serotype 13 OSE was performed. The spectrum afforded the molecular ion $[M+Na]^+$ at *m/z* 859, together with the characteristic mass increments in the series of glycosyloxonium ions formed on fragmentation at *m/z* 240, 400, 546, and 692 from the *N*-acylated Hex to 6-d-Tal, and at *m/z* 190, 336, 482, and 642 from 6-d-Tal to *N*-acylated Hex (Fig. 2A). In comparison, the fragment patterns of the cleaved terminal *N*-acylated Hex of the OSEs were *m/z* 254 and 628 in serotype 7 and *m/z* 254 and 642 in serotype 12, and those next to the terminal Hex were *m/z* 400 and 482 in serotype 7 and *m/z* 414 and 482 in serotype 12 (Fig. 2B and C). Together with the intact molecular weight of each GPL (Fig. 1B), these results strongly implied that serotype 13 GPL has no *O*-methyl group in the terminal *N*-acylated Hex but does have an *O*-methyl group added to the Rha next to the terminal Hex.

Carbohydrate composition and linkage analyses. GC/MS analysis of the perdeuteromethylated alditol acetate derivative from serotype 13 OSE was performed to determine the glycosyl composition. The total ion chromatography (TIC) of the GC/MS spectrum of serotype 13 GPL derivatives was compared to those of serotype 7 and 12 GPL derivatives (Fig. 3A). Previous reports showed that the carbohydrate compositions of the serotype 7 GPL were 6-d-Tal, Rha, and 4-2′-hydroxypropanoyl-amido-3,6-dideoxy-2-*O*-Me-Hex, and those of the serotype 12 GPL were 6-d-Tal, Rha, 4-*O*-Me-Rha, and 4-2′-hydroxypropanoyl-amido-3,6-dideoxy-3-*O*-Me-Hex (5, 13). Comparison of the retention times and mass spectra of GC/MS determined that serotype 13 GPL was composed of 6-d-Tal, Rha, 4-*O*-Me-Rha, and another terminal *N*-acylated Hex. As shown in Fig. 3B, the perdeuteromethylated alditol acetate derivative of the terminal *N*-acylated Hex was assigned to 2,3-di-*O*-deuteromethyl-1,5-di-*O*-acetyl-4-2′-*O*-deuteromethyl-propanoyl-deuteromethylamido-4,6-dideoxy-hexitol from the fragment pattern (*m/z* 62, 108, 121, 168, 209, 222, 269, and 303). These results confirmed that the *O*-methyl group was deleted from the terminal *N*-acylated Hex and added to the C-4 position at Rha next to the terminal Hex. Taken together, these results established the sequence and linkage arrangement of 4-2′-hydroxypropanoyl-amido-4,6-dideoxy-Hex-(1→3)-4-*O*-Me-Rha-(1→3)-L-Rha-(1→3)-L-Rha-(1→2)-6-d-Tal exclusively.

NMR analysis of serotype 13 OSE. The ^{1}H NMR and ^{1}H-^{1}H homonuclear COSY analyses of the OSE derived from the serotype 13 GPL revealed four distinct anomeric protons with corresponding H1-H2 cross-peaks in the low-field region at δ4.88, 4.71, 4.97 (J_{1-2} = 1 to 2 Hz, indicative of α-anomers), and 4.52 (a doublet, J_{1-2} = 7.9 Hz, indicative of a β-hexosyl unit). When further analyzed by ^{1}H-detected [^{1}H-^{13}C] two-dimensional HMQC, the anomeric protons resonating at δ4.88, 4.71, 4.97, and 4.52 had C-1s resonating at δ102.10, 93.50, 94.00, and 103.40, respectively. The J_{CH} values for each of these protons were calculated to be 170, 170, 171, and 161 Hz by measurement of the inverse-detection nondecoupled two-dimensional HMQC (see Fig. S1 and Table S1 in the supplemental material). It was concluded that two Rha and

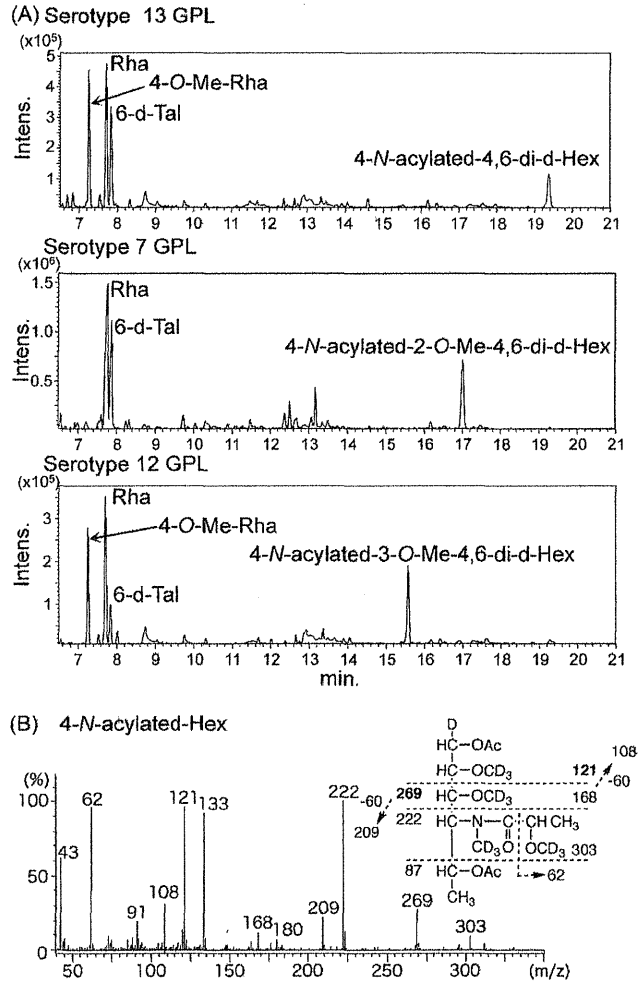

FIG. 3. Assignment of glycosyl composition of OSEs in serotype 13 GPL. (A) Total ion chromatogram of the alditol acetate derivatives from serotype 13 compared to those of serotype 7 and 12 GPLs. A fused SP-2380 capillary column was used as the GC column. The temperature program for alditol acetate derivatives was started at 60°C, increased to 40°C/min to 220°C, and held for 15 min, followed by an increase of 10°C/min to 260°C and holding for 10 min. (B) GC/MS spectrum of the perdeuteromethylated alditol acetate derivative from the terminal Hex in serotype 13 GPL. The pattern of prominent fragment ions is illustrated. A fused Equity-1 capillary column was used as the GC column. Ac, CH_3CO.

4-*O*-Me Rha were α-anomers and that the terminal *N*-acylated Hex was a β configuration.

Nucleotide sequence of *orfA-orfB* region of *M. intracellulare* serotype 13. The present study demonstrated that the difference between the chemical structures of the serotype 13 GPL and serotype 7 and 12 GPLs was whether the *O*-methyl group in the terminal *N*-acylated Hex and the next Rha were present or not. We confirmed the genetic basis of these *O*-methylations. Our previous study clarified three unique open reading frames (ORFs) for methyltransferase, named *orf2*, derived from *M. intracellulare* serotype 7, and *orfA* and *orfB*, from *M. intracellulare* serotype 12 (13, 30). *orfA* and *orfB* in *M. intracellulare* serotype 12 are responsible for 4-*O*-methylation of the Rha next to the terminal Hex and 3-*O*-methylation of the

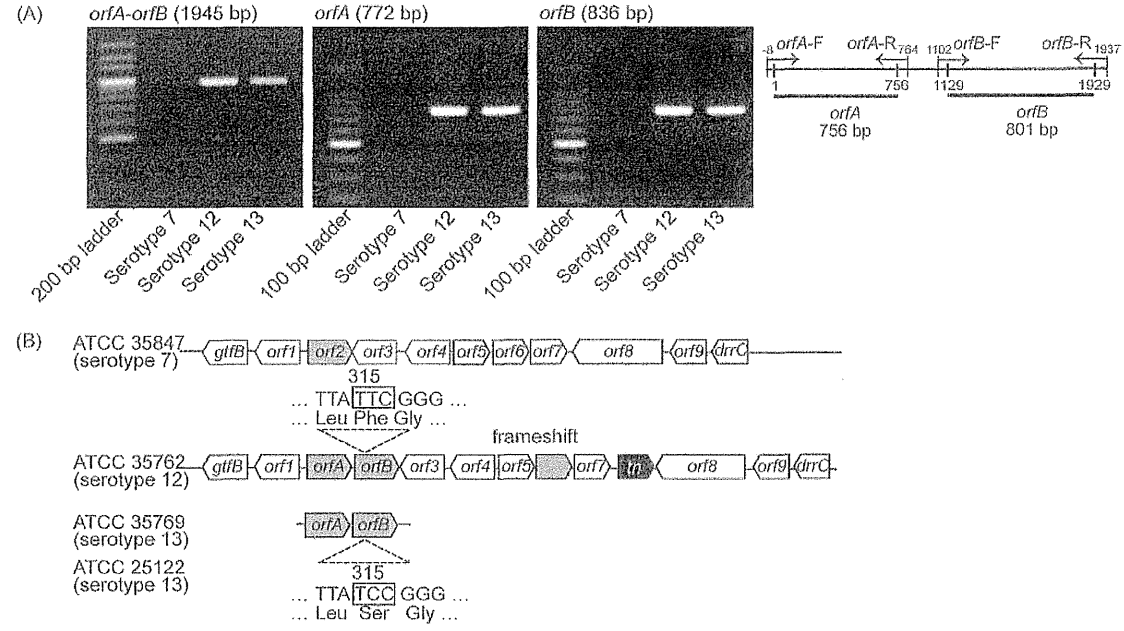

FIG. 4. Detection of *orfA-orfB* regions and comparison of genetic maps of GPL biosynthetic cluster. (A) PCR was performed to amplify the *orfA-orfB* regions of *M. intracellulare* serotype 7, 12, and 13 strains. The primers and the amplified regions are indicated. (B) *M. intracellulare* serotype 7 ATCC 35847 and serotype 12 ATCC 35762 were sequenced in our previous work (13, 30). *M. intracellulare* serotype 13 ATCC 35769 and ATCC 25122 were sequenced in this study. The missense mutation of *orfA-orfB* regions is indicated.

terminal Hex, respectively. Therefore, we examined whether or not *M. intracellulare* serotype 13 has these ORFs. First, comparison of the *gtfB-drrC* gene cluster in *M. intracellulare* serotype 7 and 12 strains implied that *orf2* in *M. intracellulare* serotype 7 replaced *orfA-orfB* in *M. intracellulare* serotype 12. We amplified the *orfA-orfB* in the genomic DNA from *M. intracellulare* serotypes 7, 12, and 13 (Fig. 4A). Interestingly, *M. intracellulare* serotype 13 had the same-sized DNA fragment of the *orfA-orfB* region, and the nucleotide sequences were determined. The 1.95-kb *orfA-orfB* regions of the two serotype 13 strains had complete identity and showed only one nucleotide substitution from that of serotype 12: codon 105, TTC, of the *orfB* in serotype 12 was replaced by codon TCC in serotype 13 (Fig. 4B). This missense mutation induced a single amino acid substitution from Phe to Ser and implied the loss of the *orfB* activity for *O*-methylation.

Expression of sero12-*orfB* and sero13-*orfB* in *M. intracellulare* serotype 13. To test the functional activity of *orfB* in *M. intracellulare* serotypes 12 and 13, the sero12-*orfB* and sero13-*orfB* genes were introduced into the *M. intracellulare* serotype 13 strain. The 0.84-kb sero12-*orfB* and sero13-*orfB* were amplified and cloned into a pVV16 vector, and *M. intracellulare* serotype 13 ATCC 35769 was transformed with the resulting plasmids and the pVV16 vector. The alkaline-stable lipids derived from the transformants were developed on TLC plates, and the productive GPLs were compared to the spots of serotype 7, 12, and 13 GPLs (Fig. 5A). Both R_f values of the GPLs produced in the transformants with the pVV16 vector and sero13-*orfB* were identical to that of the serotype 13 GPL. However, the R_f value of the GPL produced in the transformant with sero12-*orfB* was the same as that of serotype 12 GPL. By MALDI-TOF MS, the main molecular weights of the GPLs produced in the transformants with sero12-*orfB*, sero13-*orfB*, and the pVV16 vector were detected as *m/z* 1,911, 1,897, and 1,897, respectively, for $[M+Na]^+$ (data not shown). The fragment ions of the related glycosyl cleavage in the OSEs were analyzed by using MALDI-TOF MS/MS, and the glycosyl compositions were determined. The fragment ions of the OSEs in the pVV16 vector and sero13-*orfB* showed the same pattern as serotype 13 GPL, indicating that overexpression of sero13-*orfB* in the serotype 13 strain was not affected (Fig. 2A and 5B). The fragment ions of the OSE in sero12-*orfB*, i.e., *m/z* 254 and 414, were different from those of the OSE in sero13-*orfB*, i.e., *m/z* 240 and 400, respectively (Fig. 5B). The GC/MS spectrum of the perdeuteromethylated alditol acetate derivative of the terminal *N*-acylated Hex from sero12-*orfB* was assigned to 2-*O*-deuteromethyl-1,5-di-*O*-acetyl-4-2′-*O*-deuteromethyl-propanoyl-deuteromethylamido-4,6-dideoxy-3-*O*-methyl-hexitol from the fragment pattern (*m/z* 62, 105, 121, 165, 206, 222, 266, and 300) (Fig. 5C), which was identical to that of the serotype 12 GPL. These results demonstrated that the serotype 13 transformant with sero12-*orfB* but not sero13-*orfB* had an added *O*-methyl group at the C-3 position in the terminal Hex and that the productive GPL was completely changed from serotype 13 to serotype 12. In addition, we confirmed that the plasmid-deleted C-terminal 40-base region of sero12-*orfB* was completely functional and that sero12-*orfB* worked in the serotype 7 transformant. Taken together, these results indicated that sero13-*orfB* was inactivated by the missense mutation at codon 105 and that the serotype 13 GPL lacked *O*-methylation at the C-3 position of the terminal Hex.

Native conformation of serotype 13 GPL and host response. The native serotype 13 GPL was purified without alkaline treatment. The native serotype 13 GPLs were detected on TLC

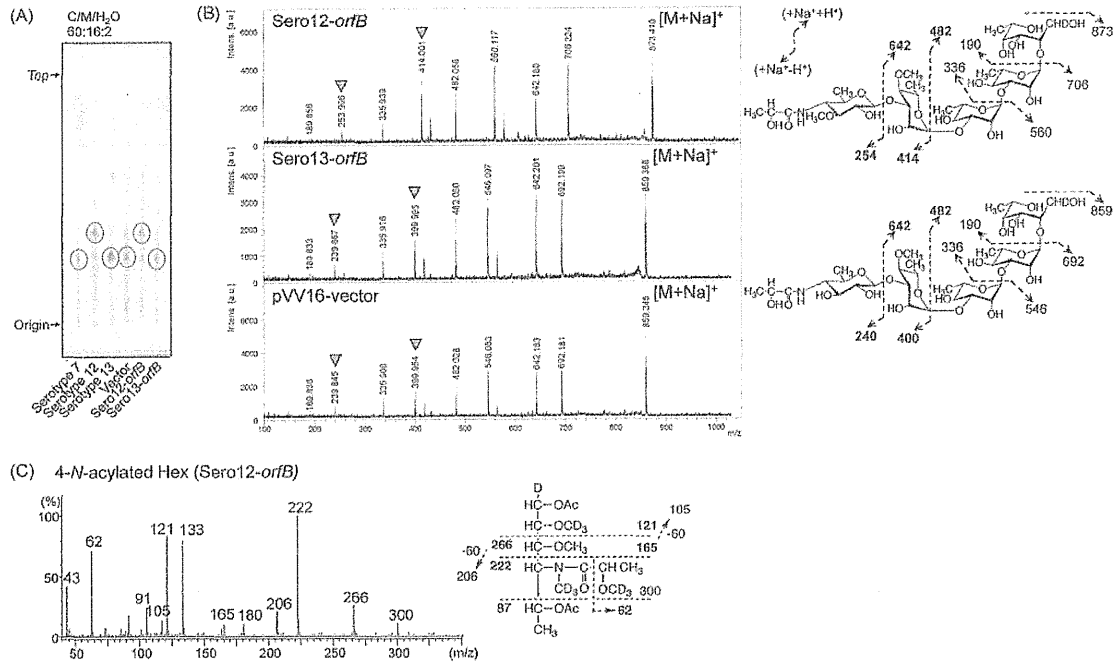

FIG. 5. The productive GPLs in transformants of *M. intracellulare* serotype 13 with sero12-*orfB* or sero13-*orfB*. (A) TLC patterns of the alkaline-stable lipids derived from *M. intracellulare* serotypes 7, 12, and 13 and serotype 13 transformants (ATCC 35769) with the pVV16-vector, sero12-*orfB*, and sero13-*orfB* from left to right, developing with a solvent system of chloroform-methanol-water (60:16:2 [vol/vol/vol]). (B) MALDI-TOF MS/MS spectra of OSEs derived from the productive GPLs in transformants of *M. intracellulare* serotype 13 with sero12-*orfB*, sero13-*orfB*, and the pVV16 vector. The replaced mass numbers are indicated by arrowheads. (C) GC/MS spectrum of the perdeuteromethylated alditol acetate derivative of the terminal *N*-acylated Hex from serotype 13 transformant with sero12-*orfB*. The MALDI TOF MS/MS and GC/MS conditions are described in the legends for Fig. 2 and 3. Ac, CH_3CO.

plates as three major spots that expanded broadly and had R_f values different from that of the alkaline-treated serotype 13 GPL. These spots were converged into one spot by alkaline treatment (Fig. 6A). It was reported that some positions of OSE in GPLs are acetylated in nature (27). The molecular weights of these three spots were checked by MALDI-TOF MS. The mass numbers of *m/z* 1,983, 2,025, and 2,067 for $[M+Na]^+$ caused the 2- to 4-unit increases of *m/z* 42 (addition of acetylations) and the modification to saturated alkyl group, compared to *m/z* 1,897 of the alkaline-treated serotype 13 GPL, implying that native GPLs were modified by several *O*-acetylations in the OSE portion and that alkaline treatment removed the acetylated groups (Fig. 6B). In addition, several peaks at intervals of 14 atomic mass units were caused by an alkyl group, indicating that the fatty acids of the core portion were variable and that the molecular species were heterogeneous.

To clarify the host recognitions of serotype 13 GPL via TLRs, we stimulated HEK-blue-2 and -4 cells with native and alkaline-treated serotype 13 GPLs. The native serotype 13 GPL significantly activated HEK-blue-2 cells in a dose-dependent manner, but HEK-blue-4 cells did not respond. The alkaline-treated serotype 13 GPL without *O*-acetylation did not activate either HEK-blue-2 or -4 cells. Reacetylated alkaline-treated serotype 13 GPLs with *O*-acetyl groups substituted for all hydroxy groups of OSE activated HEK-blue-2 cells, although the level of activation was less than that of the native form (Fig. 6C). Moreover, we confirmed that only the native serotype 13 GPL stimulated mouse bone marrow-derived macrophages via TLR2 by using C57BL/6 and TLR2 knockout mice (see Fig. S2 in the supplemental material).

DISCUSSION

The structural heterogeneity of the GPLs in MAIC species is reflected in their morphology, virulence, and pathogenicity (2, 3, 24) and may be meaningful in phylogenetic classification. Actually, epidemiological studies show that the isolates of MAIC serotypes from patients are heterogeneous and important for assessing the prognosis of pulmonary MAIC disease (25, 37). Chatterjee and Khoo (9) proposed grouping the three types of GPLs by OSE structure, and the group 2 GPLs included the serotype 12, 17, and 19 strains. The serotype 7 and 16 GPLs determined in our previous studies also belong to the group 2 GPLs (13, 14). The group 2 GPLs have in common 6-d-Tal-Rha-Rha and serotype-individual sugars elongated from the second Rha. In addition, except for the serotype 19 GPL, group 2 GPLs carry an unusual substituent, *N*-acylated amido sugar, as the terminal Hex. Aspinall et al. (1) mentioned that the terminal sugar residue of serotype 12 GPL is a derivative of viosamine (4-amino-4,6-dideoxyglucose). The structural difference between serotype 7 and 12 GPLs in group 2 was due to the functions of three methyltransferase genes, *orf2*, *orfA*, and *orfB* (13, 30). In this study, we found that the serotype 13 GPL was structurally very close to those of serotypes 7 and 12, and we determined the novel structure of

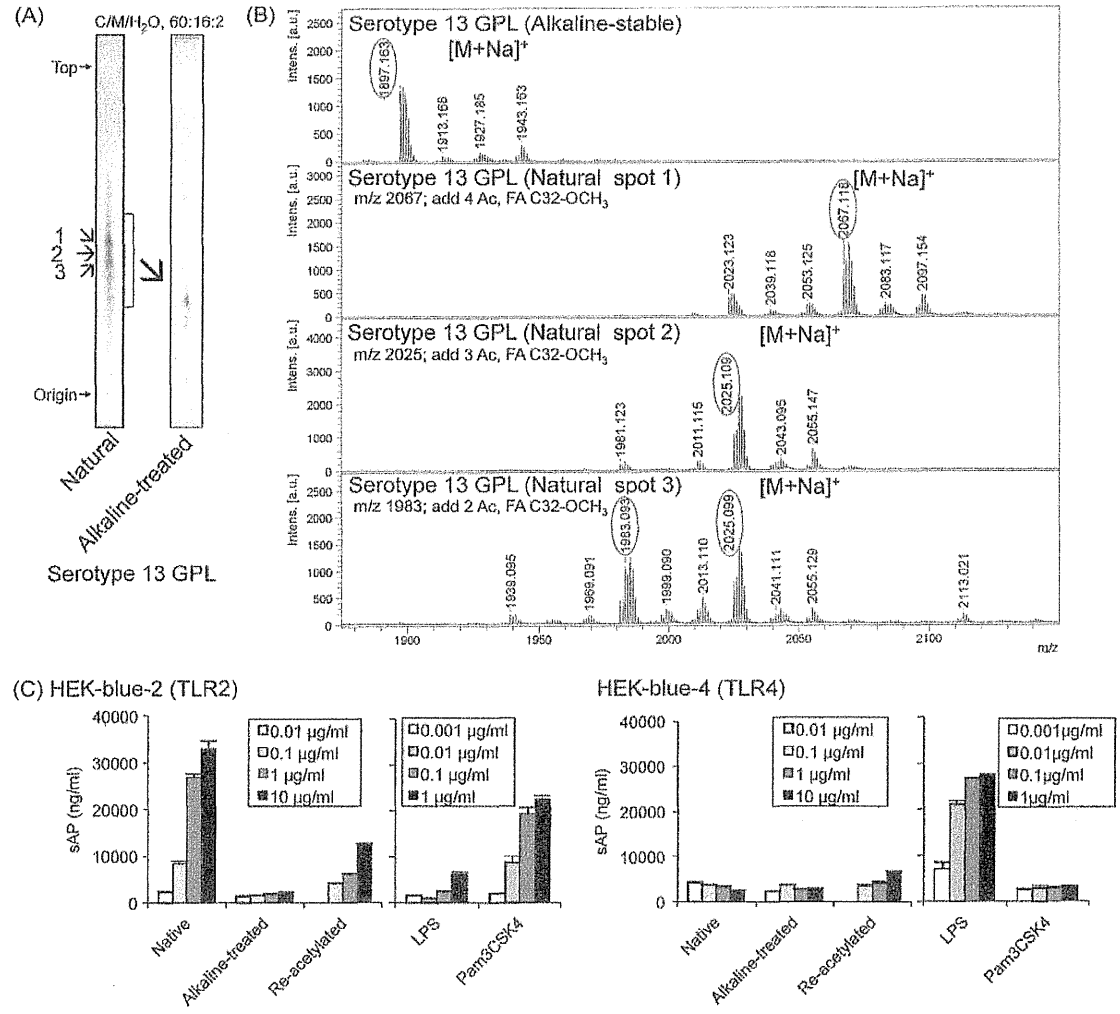

FIG. 6. TLC patterns, MALDI-TOF MS spectra, and TLR recognition of the native and alkaline-treated serotype 13 GPL. (A) The TLC plate was developed with a solvent system of chloroform-methanol-water (60:16:2 [vol/vol/vol]). Three major spots of native GPL are indicated by the numbers from top to bottom. (B) The major spots were purified and their molecular ions were measured by MALDI-TOF MS. The condition is described in the legend for Fig. 1. (C) HEK-blue-2 and -4 cells (2×10^5 cells/ml) were stimulated with native, alkaline-treated, and reacetylated serotype 13 GPLs. After 24 h of incubation, NF-κB activation was assessed by measuring the levels of secreted alkaline phosphatase (sAP) in the supernatant by using QUANTI-Blue. The data are means ± standard deviations (SD) for two experiments done in duplicate.

the serotype 13 GPL to be 4-2′-hydroxypropanoyl-amido-4,6-dideoxy-β-hexose-(1→3)-4-*O*-methyl-α-L-rhamnose-(1→3)-α-L-rhamnose-(1→3)-α-L-rhamnose-(1→2)-α-L-6-deoxy-talose. This result clarified that the serotype 13 GPL is structurally different from the serotype 7 and 12 GPLs in the *O*-methylations of the terminal *N*-acylated Hex and Rha next to the terminal Hex. Serotype 13 GPL lacked the *O*-methyl group in the terminal *N*-acylated Hex, although serotype 7 and 12 GPLs had one at the C-2 and C-3 positions, respectively. The composition and position of the *N*-acyl group at the terminal Hex were completely identical in these three GPLs. At the Rha next to the terminal Hex, serotype 12 and 13 GPLs have an *O*-methyl group at the C-4 position, and this modification is present in all group 2 GPLs except for the serotype 7 GPL, suggesting that this methyl group may play a role in MAIC physiology and virulence. These results also implied that *M. intracellulare* serotypes 7, 12, and 13 are very close phylogenetically.

We investigated the relationship between the structure and biosynthetic pathway and tried to verify the phylogenetic classification of serotypes 7, 12, and 13 by genetic analysis of GPL biosynthesis. We previously reported the nucleotide sequences of the *gtfB-drrC* region, which completely determine each serotype-specific GPL in serotypes 7 and 12 (13, 30), and found the sequence of the serotype 13 gene cluster (unpublished data). The genetic organizations of the *gtfB-drrC* regions in serotype 7, 12, and 13 gene clusters closely resemble each other. Seven common ORFs are conserved in *gtfB-drrC* clusters, suggesting that these three serotypes diverged from a common ancestor. The *orfA-orfB* region in serotypes 12 and 13 replaced *orf2* in serotype 7. Only one nucleotide substitution was found in the 1.95-kb segment in *orfA-orfB* of serotypes 12

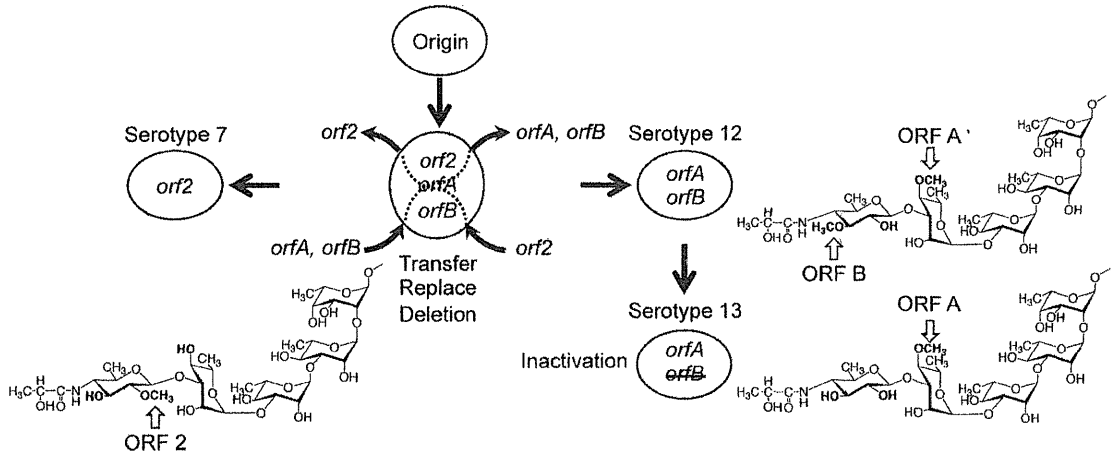

FIG. 7. Scheme of the relationship between GPL biosynthesis ORFs encoded the methyltransferases and their structures.

and 13, and *orfB* in serotype 13 was inactivated. In general, it is unusual for an ORF inactivated by a missense mutation to remain in the genome because it is a burden for the bacterium to transcribe and translate an inactivated ORF. Thus, the *M. intracellulare* serotype 13 strain must have diverged from an *M. intracellulare* serotype 12 organism recently. Serotype 13 GPL also has 4-*O*-Me-Rha. *orfA* is responsible for this methylation. In previous studies, we demonstrated that the *orfB* activity had incapacitated the *orf2* activity, which synthesizes an *O*-methyl group at the C-2 position of the terminal Hex of *M. intracellulare* serotype 7. We also showed that the *orf2* activity was independent of *orfA* activity in *M. intracellulare* serotype 12 (30). The relation of methyltransferases, *orfA*, *orfB*, and *orf2* is summarized in Fig. 7.

GPLs are correlated with colony morphology, sliding motility, biofilm formation, immune modulation, and virulence (2, 3, 16, 34). GPLs have several significant features. They are produced in MAIC species and absent from *Mycobacterium tuberculosis*, making it possible to distinguish MAIC from tuberculous mycobacteria (11, 20). An anti-GPL antibody is produced in the sera of patients and reflects the disease, which is useful in diagnosis and treatment (21, 22, 25). Moreover, it was reported that ethambutol-susceptible and -resistant MAIC strains of serotype 1 had different GPL profiles. The susceptible strain expressed only the polar serotype 1 GPL, and the resistant strain expressed several apolar GPLs. The efficacy of antibiotics may be affected by the GPL profile through differences in cell wall permeability (19). On the other hand, the importance of TLR-mediated responses has been studied in tuberculous infections. Means et al. (28) reported that *M. tuberculosis* activated both TLR2 and TLR4, whereas heat-killed *M. tuberculosis* and *M. avium* activated only TLR2. It was observed that MyD88- and TLR2-deficient mice have increased susceptibility to *M. avium* infection compared to TLR4-deficient and wild-type mice (12). These lines of evidence suggest that TLRs are related to host recognition of the MAIC components containing GPLs and affect MAIC infections. Brennan and Goren (6) first proposed that GPLs were alkaline-stable lipids and made it possible to classify serospecificity by the unique, variable deacetylated OSE sequences (9). We did not detect any biological activity of these alkaline-treated GPLs on splenocytes and bone marrow macrophages of mice in *in vitro* stimulation. Recently, Schorey and colleagues (35, 36) clarified that serotype 1 and 2 GPLs can function as TLR2 agonists and promote macrophage activation in a TLR2- and MyD88-dependent pathway. They reported that the acetylated and methylated groups of GPLs were necessary for GPL-TLR2 interaction as a molecular requirement. In this study, we purified both native and alkaline-treated serotype 13 GPLs and clarified the acetylation patterns of serotype 13 GPL. It was confirmed that the native acetylated form of serotype 13 GPL was recognized via TLR2 and that the deacetylated form by alkaline treatment was not recognized. The serotype 13 GPL has one *O*-methyl group next to the terminal *N*-acylated Hex that was stable regardless of alkaline treatment. Taken together, an acetyl rather than a methyl group was necessary for host immune response via TLR2. The completely acetylated derivative of alkaline-treated serotype 13 GPL partially recovered the HEK-blue-2 activation, compared to the native form containing 2 to 4 acetylated groups. It may be important for GPL-TLR2 interaction to balance the hydrophobicity and hydrophilicity of the molecule. Recht and Kolter (32) reported that the acetylation of GPL affects sliding motility and biofilm formation by deleting the *atf1* gene, which is responsible for acetylation on the 6-d-Tal of GPL core in *Mycobacterium smegmatis*. Rhoades et al. (33) reported that the *Mycobacterium abscessus* GPLs were related to smooth and rough colony morphology and that the GPLs in the outermost portion of the cell wall masked underlying phosphatidyl-*myo*-inositol mannosides involved in stimulating the innate immune response via TLR2. In contrast, our results suggest that the species-specific acetylated GPL is effective in host recognition as a TLR2 agonist independent of phosphatidyl-*myo*-inositol mannosides and that it plays important roles directly in host innate immune responses. Regulating the acetylation of GPL may control the MAIC pathogenicity by, for example, developing the inhibitor of ATF1.

The present study demonstrated the chemical structure and biosynthesis gene cluster of the serotype 13 GPL of *M. intracellulare* and host innate immune response via TLR2. Serotype 13 GPL should be included in group 2 GPLs, and the phylogenetic relationship of serotype 7, 12, and 13 strains was par-